

SINGLE ION CONDUCTORS BASED ON POLYMER-MODIFIED
NANOPARTICLES: SYNTHESIS AND CHARACTERIZATION

By

Hui Zhao

A THESIS

Submitted to
Michigan State University
in partial fulfillment of the requirements
for the degree of

MASTER OF SCIENCE

Chemistry

2012

ABSTRACT

SINGLE ION CONDUCTORS BASED ON POLYMER-MODIFIED NANOPARTICLES: SYNTHESIS AND CHARACTERIZATION

By

Hui Zhao

Lithium ion battery has been widely used nowadays. Occurrence of polarization has been a problem in the currently used electrolyte, especially in high-current application such as hybrid vehicles. In this work we modified silica nanoparticles with polyelectrolytes containing anion groups, lithium cation is the counterion. To get the lithium conductor, the polymer modified nanoparticles were blended with poly(ethylene oxide) oligomer. Movement of the anions were largely restricted by surface anchored polymer backbones, lithium ion became the only ion that is conducting current.

Four different polymer structures were explored in this study, aiming at improving conductivity of the material. FTIR and TGA were used to prove successful synthesis of the polymer modified particles. AC impedance was used to measure the conductivity.

ACKNOWLEDGEMENTS

I would like to thank my advisor Professor Gregory Baker, who was always patient and taught me all the basic knowledge of polymer synthesis. Many thanks to my guidance committee, Dr. William Wulff, Dr. Mitch Smith and Dr. Merlin Bruening, for helpful discussions.

Many thanks to Dan Holmes, Rui Huang, Kathy Severin, Alacia Pastor for teaching me different characterizing techniques. I would like to thank past and current group members Qin, Sampa, Erin, Tom, DJ, Gina, Quanxuan, Wen, Heyi, Yiding, Zhe and Greg. They are wonderful labmates and I enjoyed doing research with them.

Last but not least, none of this would be possible without my Mom and Dad. They have been very supportive and patient along the way. This thesis is dedicated to my parents.

TABLE OF CONTENTS

LIST OF TABLES	V
LIST OF FIGURES	VI
LIST OF SCHEMES	IX
LIST OF ABBREVIATIONS	XI
1. Introduction.....	1
1.1 Lithium Ion Batteries.....	1
1.2 Polymer Electrolytes	6
1.3 Conductivity Measurements.....	10
1.4 Lithium Transference Number	15
1.5 Electrolytes with High t_{Li^+} in Literature.....	18
2. Results and Discussion	27
2.1. Particles Modified with Lithium 4-Styrenesulfonate.....	29
2.2. Particles Modified with Lithium 4-Styrenesulfonate and PEGMA.....	37
2.3. LiTFSI Analogue Polymer Modified Particles.....	44
2.4. Phosphonic Acid Modified Particles	53
3. Conclusions	60
4. Experimental Section.....	61
5. References	71

LIST OF TABLES

Table 1. Conductivities of lithium salts used in lithium ion battery research	3
Table 2. Examples of synthetic lithium salts	5
Table 3. Typical polymer electrolytes and their conductivities	10
Table 4. Weight content of LiTFSI in LiTFSI/PEGDME-500 at various O/Li ratios (2.4×10^{-2} g Li/ g LiTFSI)	14
Table 5. Lithium transference numbers for typical lithium salts	16
Table 6. Particle weight content for electrolytes prepared from Si-PSSLi (2.4×10^{-2} g Li/g nanoparticles) dispersed in PEGDME-500.....	35
Table 7. Particle weight fraction for Si-PSSLi-PEGMA (1.56×10^{-2} g Li/g sample) dispersed in PEGDME-500	42
Table 8. Particle weight content for electrolytes prepared from Si-TFMA-Li (2.0×10^{-2} g Li/g sample) dispersed in PEGDME-500	51
Table 9. Particle weight content for electrolytes prepared from Si-PPLi (3.45×10^{-2} g Li/g sample) dispersed in PEGDME-500	57

LIST OF FIGURES

Figure 1. A schematic diagram of a lithium ion battery using metal oxide cathode and graphite anode.....	2
Figure 2. Side and top views of the 7_2 helix of PEO.....	7
Figure 3. A typical Nyquist plot obtained from AC impedance spectroscopy.....	12
Figure 4. Temperature dependent conductivity for LiTFSI/PEGDME-500 electrolytes at various O/Li ratios.....	14
Figure 5. Conductivity vs. O/Li for LiTFSI/PEGDME-500 at various temperatures	15
Figure 6. Polarization during discharge of a lithium ion battery	18
Figure 7. TEM image of Snowtex-S silica nanoparticles (samples were dispersed in water dropped on a copper grid, and dried before taking the TEM image)	29
Figure 8. FTIR spectra of (a) Snowtex-S silica particles; (b) Si-Initiator, initiator grafted silica particles, and (c) Si-PSSLi, silica particles grafted with poly(lithium 4-styrene sulfonate).....	31
Figure 9. Thermogravimetric Analysis (TGA) curves of (a) Snowtex-S silica particles; stabilized by CTAB; (b) Si-Initiator, silica particles grafted with initiator, and (c) Si-PSSNa, silica particles grafted with poly(sodium 4-styrene sulfonate), and (d) Si-PSSLi, poly(lithium 4-styrene sulfonate) grafted silica particles.....	32
Figure 10. TEM image of Si-PSSLi (samples were dispersed in water, dropped on a copper grid, and dried before taking the TEM image).....	35
Figure 11. Temperature dependant conductivity for Si-PSSLi/PEGDME-500 at various O/Li ratios.....	36

Figure 12. Room temperature conductivity as a function of the O/Li ratio for Si-PSSLi/PEGDME-500 electrolytes	37
Figure 13. FTIR spectra of (a) Snowtex-S silica particles, stabilized by CTAB; (b) Si-Initiator, silica particles grafted with initiator, and (c) Si-PSSLi-PEGMA; silica particles grafted with poly(lithium 4-styrenesulfonate) and PEGMA	40
Figure 14. TGA curves of (a) Snowtex-S silica particles, stabilized by CTAB; (b) Si-Initiator, silica particles grafted with initiator, (c) Si-PSSNa-PEGMA; silica particles grafted with poly(sodium 4-styrenesulfonate) and PEGMA and (d) Si-PSSLi-PEGMA; silica particles grafted with poly(lithium 4-styrenesulfonate). 41	
Figure 15. TEM image of Si-PSSLi-PEGMA (samples were dispersed in water, dropped on a copper grid, and dried before taking the TEM image).....	42
Figure 16. Temperature dependant conductivity of Si-PSSLi-PEGMA/PEGDME-500 electrolytes at various O/Li ratios	43
Figure 17. Room temperature conductivity vs O/Li ratio for Si-PSSLi-PEGMA /PEGDME-500.....	44
Figure 18. FTIR spectra of (a) Snowtex-S silica particles; (b) Si-Initiator, initiator modified silica particles; (c) Si-TFMA-Li, lithiated poly(trifluoromethane sulfonic aminoethylmethacrylate) modified silica particles.....	48
Figure 19. FTIR spectra of (a) Si-TFMA, poly(trifluoromethane sulfonic aminoethylmethacrylate) modified silica particles; (b) Si-TFMA-Li, lithiated poly(trifluoromethane sulfonic aminoethylmethacrylate) modified silica particles	49
Figure 20. TGA curves of (a) Snowtex-S silica particles, stabilized by CTAB; (b) Si-Initiator, silica particles grafted with initiator, (c) Si-TFMA, poly(trifluoromethane sulfonic aminoethylmethacrylate) grafted silica particles; and (d) Si-TFMA-Li, lithiated poly(trifluoromethane sulfonic aminoethylmethacrylate) grafted silica particles	50

Figure 21. Temperature dependant conductivity of Si-TFMA-Li/PEGDME-500 electrolytes at various O/Li ratios	51
Figure 22. Room temperature conductivity as a function of the O/Li ratio for Si-TFMA-Li/PEGDME-500.....	52
Figure 23. TGA curves of (a) Snowtex-S silica particles; (b) Si-Initiator, initiator modified silica particle; (c) Si-PDEVBP, silica particle modified by poly(diethyl 4-vinylbenzylphosphonate); (d) Si-PPLi, poly(lithium 4-vinylbenzylphosphonate)	56
Figure 24. FTIR spectra of (a) Si-PDEVBP, silica particle modified by poly(diethyl 4-vinylbenzylphosphonate); (b) Si-PPLi, poly(lithium 4-vinylbenzylphosphonate)	57
Figure 25. Temperature dependent conductivity of Si-PPLi/PEGDME-500 at various O/Li ratios.....	58
Figure 26. Room temperature conductivity vs. O/Li ratio for Si-PPLi/PEGDME-500 electrolytes.....	59

Images in this dissertation are presented in color.

LIST OF SCHEMES

Scheme 1. Lithium transport mechanism in PEO described by Ratner <i>et al</i>	8
Scheme 2. Typical aza-ether and boron derivatives in McBreen's work.....	19
Scheme 3. A typical calixarene described by Wieczorek.....	19
Scheme 4. Boroxine containing polymer described by Mehta	20
Scheme 5. Two pre-polymer structures (top) and the boron crosslinker (bottom) described by Kerr	22
Scheme 6. Polysiloxane comb polymers synthesized by Shriver	23
Scheme 7. Monomers described by Endo	24
Scheme 8. Synthetic approach to polyelectrolyte-decorated nanoparticles.....	28
Scheme 9. Immobilization of initiators on silica particles and the following surface ATRP with sodium 4-styrene sulfonate	30
Scheme 10. Lithiation of silica particles grafted by poly(sodium 4-styrenesulfonate) (Si- PSSNa).....	31
Scheme 11. Quantitative determination of the Li content in nanoparticles	34
Scheme 12. Copolymerization of sodium 4-styrenesulfonate and PEGMA from silica Nanoparticles	38
Scheme 13. Method used to calculate the copolymer content in Si-PSSNa/PEGMA modified nanoparticles	39
Scheme 14. Lithiation of Si-PSSNa-PEGMA	39
Scheme 15. A trifluoromethane sulfonic aminoethylmethacrylate (TFMA) inspired by the chemical structure of LiTFSI	46

Scheme 16. Synthesis of 2-(trifluoromethanesulfonamido)ethyl methacrylate (TFMA)	46
Scheme 17. ATRP of trifluoromethane sulfonic aminoethylmethacrylate (TFMA) from silica particles	47
Scheme 18. Lithiation of Si-TFMA to Si-TFMA-Li	48
Scheme 19. Synthesis of diethyl 4-vinylbenzylphosphonate (DEVBP).....	53
Scheme 20. ATRP of diethyl 4-vinylbenzylphosphonate (DEVBP) from particle surfaces	54
Scheme 21. Lithiation procedure for poly(diethyl 4-vinylbenzylphosphonate) grafted silica	55

LIST OF ABBREVIATIONS

σ	conductivity
AC	alternating current
ATRP	atom transfer radical polymerization
Bpy	bipyridine
CTAB	etyltrimethylammonium bromide
DEVBP	diethyl 4-vinylbenzylphosphonate
DMF	N, N-dimethylformamide
DSC	differential scanning calorimetry
EtOAc	ethyl acetate
FTIR	Fourier transform infrared spectroscopy
GPC	gel permeation chromatography
LIB	Lithium Ion Batteries
LiTFSI	lithium bis(trifluoromethane sulfone)imide
ppm	parts per million
PDI	polydispersity index
PDEVBP	poly(diethyl 4-vinylbenzylphosphonate)
PEGMA	poly(ethylene glycol) methyl ether methacrylate
PEG	poly(ethylene glycol)
PEO	poly(ethylene oxide)

PEGDME-500	poly(ethylene oxide) dimethyl ether (average molecular weight 500)
PEM	proton exchange membranes
PMDETA	N, N, N', N', N''-Pentamethyldiethylenetriamine
PPOH	poly(4-vinylbenzylphosphonic acid)
PPLi	poly(lithium 4-vinylbenzylphosphonate)
PSSLi	poly(lithium 4-styrenesulfonate)
PSSNa	poly(sodium 4-styrenesulfonate)
PTFMA	poly(trifluoromethane sulfonic aminoethylmethacrylate)
PVDF	polyvinylidene fluoride
Si-PDEVBP	silica particle modified by poly(diethyl 4-vinylbenzylphosphonate)
Si-PPOH	silica particle modified by poly(4-vinylbenzylphosphonic acid)
Si-PPLi	silica particle modified by poly(lithium 4-vinylbenzylphosphonate)
Si-PSSLi	silica particle modified by poly(lithium 4-styrenesulfonate)
Si-PSSLi-PEGMA	silica particle modified by co-poly(lithium 4-styrenesulfonate)-poly(ethylene glycol) methyl ether methacrylate
Si-PSSNa	silica particle modified by poly(sodium 4-styrenesulfonate)
Si-PSSNa-PEGMA	silica particle modified by co-poly(sodium 4-styrenesulfonate)-poly(ethylene glycol)

		methyl ether methacrylate
Si-TFMA		silica particle modified by poly(trifluoromethane sulfonic aminoethylmethacrylate)
Si-TFMA-Li		silica particle modified by lithiated poly(trifluoromethane sulfonic aminoethylmethacrylate)
r.t.		room temperature
TEM		transmission electron microscopy
TFMA		trifluoromethane sulfonic aminoethylmethacrylate
TGA		thermal gravimetric analysis
T _g		glass transition temperature
TMSBr		trimethylbromosilane
TMSCl		trimethylchlorosilane
VFT		Vogle-Fulcher-Tamman

1. Introduction

1.1. Lithium Ion Batteries

Since rechargeable lithium batteries were proposed in the 1970s, the development of electrolytes appropriate for lithium ion batteries has been an active research field.¹ High energy density batteries based on lithium is attractive since it is the lightest metal (equivalent weight $M = 6.94$ g/mol, and specific gravity $\rho = 0.53$ g/cm³) and the most electropositive metal (-3.04 V versus standard hydrogen electrode). Initially, the emphasis was on batteries with metallic lithium anodes to maximize the battery capacity, but metallic lithium posed significant safety issues. To avoid the use of lithium metal, the “rocking-chair” concept² was introduced, where ions are shuttled between two interaction compounds, usually lithium intercalated graphite as the anode and a metal oxide as cathode. (Figure 1).

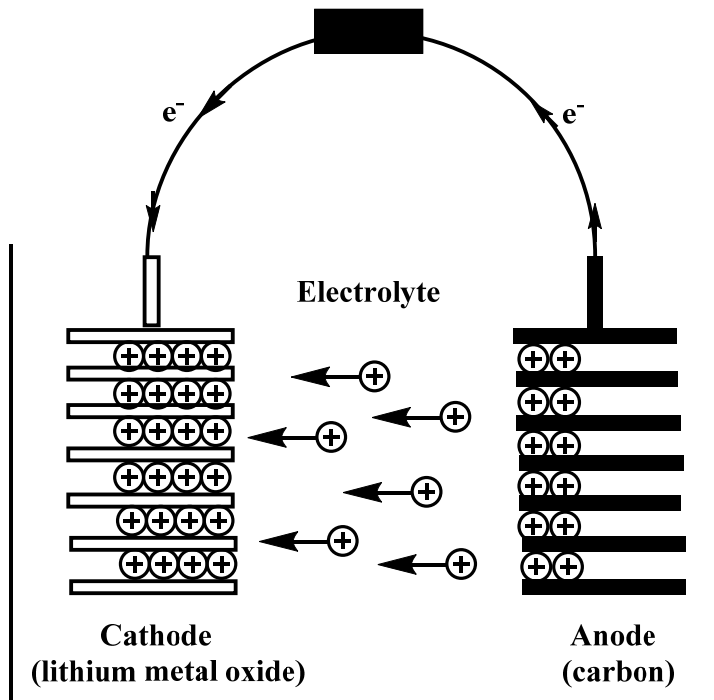


Figure 1. A schematic diagram of a lithium ion battery using metal oxide cathode and graphite anode.

Electrolytes in commercial lithium ion batteries are normally comprised of lithium salts dissolved in highly polar solvents (high dielectric constant), such as ethylene carbonate (EC), propylene carbonate (PC), dimethyl carbonate (DMC), and derivatives of tetrahydrofuran (THF). The basic requirement for a salt is that it has a low lattice energy, which results in a high degree of dissociation in the solvent. Both the salt and solvent must chemically, thermally, and electrochemically stable throughout the voltage window of the cell. Parameters of commonly used lithium salts are listed in Table 1.³

	T _m (°C)	σ (mS/cm in PC) ^a	σ (mS/cm in 1:3 EC/DMC) ^a
LiClO ₄	236	5.5	8.4
LiBF ₄	293	4.6	4.9
LiPF ₆	340	5.8	10.7
LiAsF ₆	340	5.7	11.1
LiCF ₃ SO ₃	>300	2.4	2.8
Li[N(SO ₂ CF ₃) ₂] (TFSI)	234	5.1	7.2
Li[N(SO ₂ CF ₂ CF ₃) ₂]	>350	4.4	7.8

^aAll measurements at room temperature; PC = propylene carbonate, EC = ethylene carbonate, DMC = dimethyl carbonate; all salt concentrations are 1M.

Table 1. Conductivity of lithium salts used in lithium ion battery research.³

The ionic conductivity (σ) at a specific temperature is often expressed as

$$\sigma = n \cdot q \cdot \mu$$

where n is the number of charge carriers per unit volume, q is charge of the carrier and μ is the mobility of the ions. Ion mobility is related to the degree of dissociation, ion size, charge distribution, and the degree to which ions aggregate. For lithium salts, these requirements are usually satisfied with large anions where the charge is highly delocalized. A number of such anions have been synthesized, as shown in Table 2. Most of the anions in Table 2 are large and have electron

withdrawing groups that are designed to delocalize the negative charge, decrease the electrostatic interaction between lithium cation and anion, and increase the degree of dissociation.

The use of organic solvents has some limitations. Degradation of organic solvents at electrode surfaces forms the solid-electrolyte-interphase (SEI). If the SEI is mechanically stable and has high ionic conductivity, degradation is limited to the cell's first few cycles. However, unstable SEIs can lead to consumption of the electrolyte and decreased cell capacity. Volatile degradation byproducts can cause an increase in cell pressure necessitating high-pressure packaging. Also, some electrolytes are corrosive and react with seals and containers.

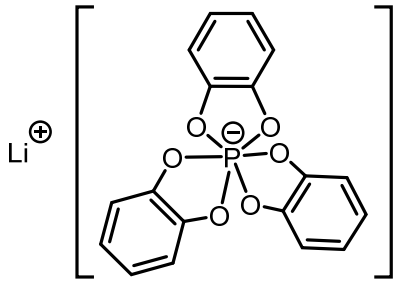
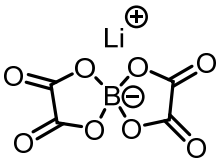
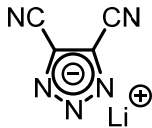
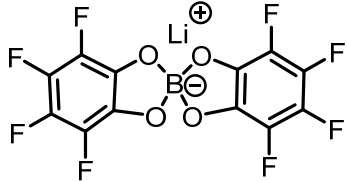
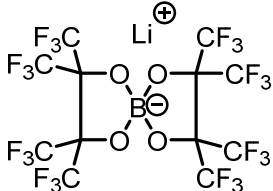
Synthetic Lithium Salt	Room Temperature Conductivity (S/cm)
	<p>1.4×10^{-3} (0.5 M in PC)</p> <p>Handa, M.; Suzuki, M.; Kanematsu, H.; Sasaki, Y. <i>Electrochem. Solid-State Lett.</i> 1999, 2, 60.</p>
	<p>14.9×10^{-3} (1 M in DME)</p> <p>5×10^{-3} (1 M in DME)</p> <p>Xu, W.; Angell, A. <i>Electrochem. Solid-State Lett.</i> 2001, 4, E1.</p>
	<p>$<10^{-5}$</p> <p>O/Li=20, in PEO (Mn=4,000,000)</p> <p>Egashira, M.; Scrosati, B.; Armand, M.; Beranger, S.; Michot, C. <i>Electrochem. Solid-State Lett.</i> 2003, 6, 71.</p>
	<p>11×10^{-3} (1 M in DME)</p> <p>Barthel, J.; Buestrich, R.; Carl, E.; Gores, H. J. <i>J. Electrochem. Soc.</i> 1996, 143, 3572.</p>
	<p>11.1×10^{-3} (0.6 M in DME)</p> <p>3×10^{-3} (1 M in PC)</p> <p>Xu, W.; Angell, A. <i>Electrochem. Solid-State Lett.</i> 2000, 3, 366.</p>

Table 2. Examples of synthetic lithium salts.

1.2. Polymer electrolytes

The use of solid electrolytes such as poly (ethylene oxide) (PEO) could address the above issues of using organic solvents. Solid-state electrolytes would eliminate the need for polypropylene or polyethylene mesh separators that required with liquid electrolytes, reducing cost and potentially increasing the energy density of the battery. Polymer electrolytes may inhibit lithium dendrite formation and provide flexibility in processability. Also, since mass transport of polymers is minimal, polymers should form robust SEIs. Wright and coworkers reported ionic conductivity for Na and K salts complexes of poly(ethylene oxide) (PEO) in 1973,⁴ but the technological importance of this solid electrolyte was not realized until 1978, when Armand described a solid state lithium cell with a PEO-based electrolyte.⁵

PEO, poly(ethylene glycol) (PEG), and poly(oxyethylene) (POE) are common names for a polymer with the same repeating unit, $-\text{OCH}_2\text{CH}_2-$. Ring opening polymerization of ethylene oxide by anionic or cationic processes provides PEO of predictable molecular weights, based on the monomer to initiator ratio. At room temperature, PEO is a waxy white solid material comprised of an amorphous and a crystalline phase. The glass transition temperature (T_g) of high molecular weight amorphous PEO is ~ -60 °C, while the crystalline phase forms a 7_2 helix (Figure 2), seven ethylene oxide repeating units completing two turns in the fiber period of

1.93 nm.⁶ The melting point (T_m) of PEO depends on the molecular weight. The T_m for high molecular weight PEO is ~ 67 °C, but as the molecular weight decreases, the PEO melting point decreases and low molecular PEO is a viscous liquid at room temperature. Also, the effect of the polymer end groups becomes more important in low molecular PEO.

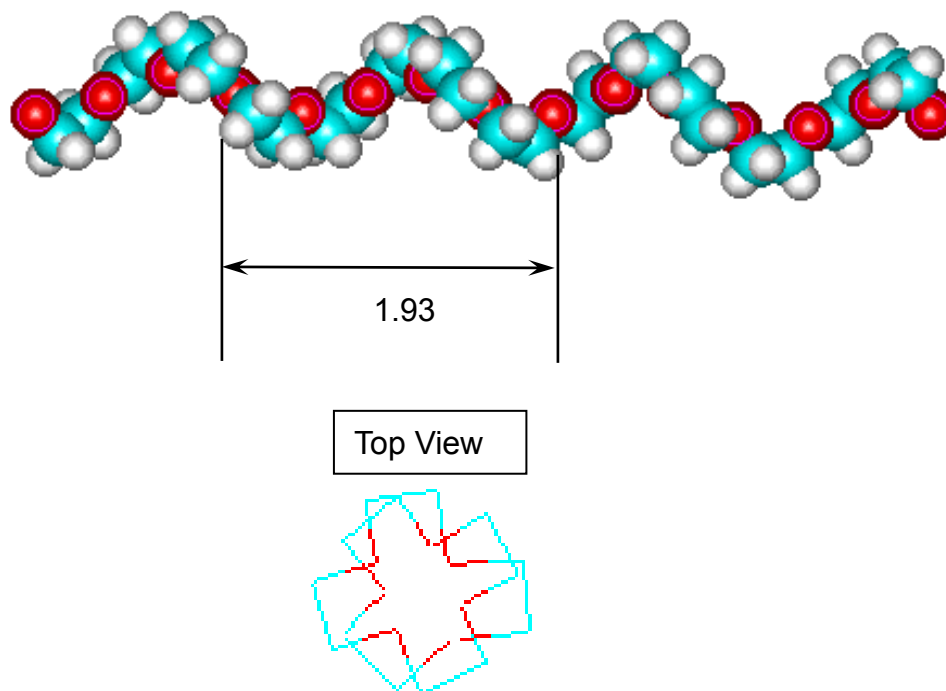


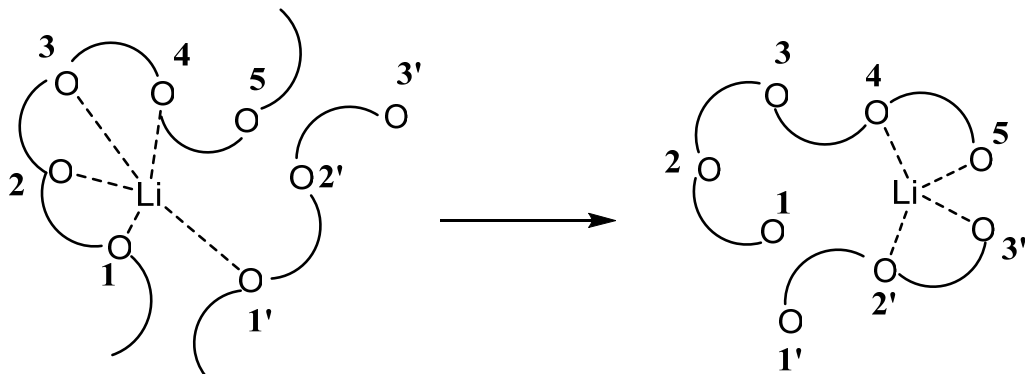
Figure 2. Side and top views of the 7₂ helix of PEO.⁶ Reprinted with permission from ref 6. Copyright 2012 American Chemical Society. (For interpretation of the references to color in this and all other figures, the reader is referred to the electronic version of this thesis.)

The generally accepted model for of Li^+ in PEO transport is that of Ratner and co-workers. Lithium cations coordinate to the lone pairs of electrons in oxygen

atoms, forming a 4-8 oxygen chelate. When an external voltage is applied, lithium ions hop to a neighboring chelation site, leading to a net flow of charge (Scheme 1.). Because the movement of ions is directly coupled to polymer chain mobility, this behavior is thermally activated and is often described by Vogel-Tammann-Fulcher (VTF) equation⁸⁻¹⁰

$$\sigma_0 = \sigma_0 \exp(-E_a / (T - T_0))$$

where σ_0 is the pre-exponential factor related to number of charge carriers, E_a is the apparent activation energy for ion transport, and T_0 is a parameter related to chain mobility of the polymer. For polymers, low T_0 s should correlate to fast relaxation and high conductivity. Since meaningful lithium transport is limited to the amorphous regions, the research described in this thesis used poly (ethylene oxide) dimethyl ether ($M_n = 500$) as a model for PEO.



Scheme 1. Lithium transport mechanism in PEO described by Ratner et al.⁷

The ionic conductivity of solid polymer electrolytes such as PEO/LiClO₄ or PEO/LiTFSI (Lithium Bis(trifluoromethane sulfonyl)imide) are 10⁻⁷-10⁻⁵ S/cm at

room temperature, several orders of magnitude lower than conventional liquid electrolytes (0.001-0.1 S/cm). The low conductivities should be expected since ion mobility is coupled to polymer chain mobility. To obtain high conductivity in “polymer-like” materials, gel polymer electrolytes were developed where a liquid electrolyte is encapsulated in a non-conducting polymer host. These two-phase materials appear to be solid state electrolytes but have the conductivity of liquid electrolytes.

Alternatives to PEO have been synthesized, and representative examples are shown in Table 3. Oxygen or nitrogen atoms are included in these polymers to provide suitable sites for Li^+ coordination, and branching is often used to prevent crystallization. Using low T_g polymer backbones such as phosphazenes and siloxanes tends to enhance conductivity. Polymethacrylates and acrylates comb architectures also have low T_g s when the “teeth” are PEG side chains.

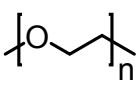
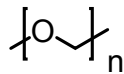
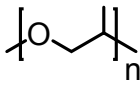
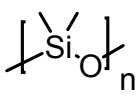
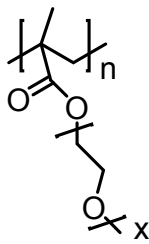
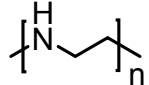
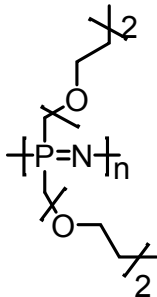
Polymer Host	Repeat Unit	Polymer Electrolyte	Conductivity (S/cm), 20 °C
poly(ethylene oxide) (PEO)		(PEO) ₈ -LiClO ₄	10 ⁻⁸
poly(oxymethylene) (POM)		(POM)-LiClO ₄	10 ⁻⁸
poly(propylene oxide) (PPO)		(PPO) ₈ -LiClO ₄	10 ⁻⁸
poly(dimethyl siloxane) (PDMS)		DMS-LiClO ₄	10 ⁻⁴
poly[methoxy poly(ethylene oxide) methacrylate]		PMG ₂₂ -LiCF ₃ SO ₃ EO:Li = 18:1	3*10 ⁻⁵
poly(ethylene imine) (PEI)		PEI-LiClO ₄	10 ⁻³
poly[bis-2-(2-methoxyethoxy) ethoxyphosphazene] (MEEP)		(MEEP) ₄ -LiBF ₄	2*10 ⁻⁵
		(MEEP) ₄ -LiTFSI	5*10 ⁻⁵
		(MEEP) ₄ -LiC(CF ₃ SO ₂) ₂	10 ⁻⁴

Table 3. Typical polymer electrolytes and their conductivities.¹¹

1.3. Conductivity measurements

Ohm's law describes the potential (E) as a function of current (I) and resistance (R)

$$E = IR$$

It is known that in a bounded area with area A (in cm^2) and length l (in cm) the resistance is defined as

$$R = \rho l / A$$

Where ρ is the resistivity of the electrolyte material in Ωcm , and

$$\rho = R(A / l)$$

conductivity σ is the reciprocal of resistivity

$$\sigma = 1 / \rho$$

so

$$\sigma = l / RA$$

unit of conductivity σ is $1 / \Omega\text{cm}$, which is S/cm (S represents Siemens).

Ionic conductivity of polymer electrolytes (or polyelectrolytes) was measured using Alternating Current (AC) Impedance Spectroscopy. In direct current (DC) circuit, resistance was used to describe the ability of circuit to resist the flow of electrical current; impedance extended this concept to AC circuit. In a real AC Impedance experiment, the electrolyte material was sandwiched between two electrodes, a sinusoidal voltage was applied to this sample cell, a sinusoidal current would be correspondingly detected. Frequency of the applied voltage ranged from 5 mHz to 1.3 MHz in this work. The sample cell here (including electrolyte material and two electrodes) responded to the applied AC voltage by generating a current, which was contributed from two parts: electrolyte material itself (as a resistor), and the interface between electrolyte and electrode (as a

capacitor). Since electrodes used to build up the sample cell are much more conductive than the electrolyte material, resistance of electrodes was ignored. If there was only resistor in this circuit, the resulting current would always be in phase with the applied sinusoidal voltage, and the magnitude of the impedance was given by resistance, which is independent of frequency; if there was only capacitor in the circuit, voltage lags behind the current by 90° . For the convenience of calculation, impedance could be expressed as a complex

$$Z = Z' - jZ''$$

Z' is the real part ($Z' = Z \cos \theta$), Z'' is the imaginary part ($Z'' = Z \sin \theta$) and j is the imaginary symbol. When data were plotted using X axis as real part, Y axis as

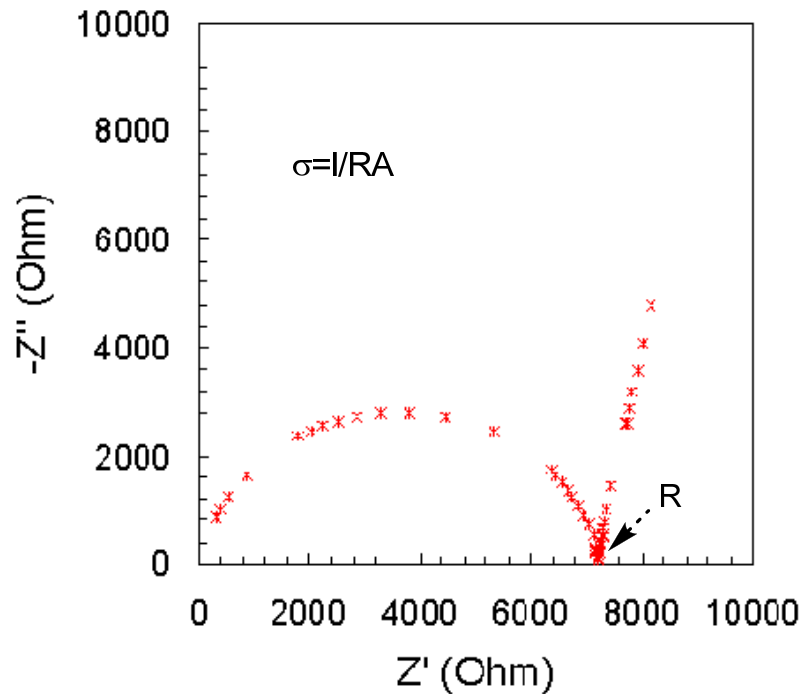


Figure 3. A typical Nyquist plot obtained from AC impedance spectroscopy.

imaginary part, the diagram was called a Nyquist plot. Frequency was not included in Nyquist plot, which was a major shortcoming. The bulk resistance of material (R in Ω) could be obtained from the Nyquist plot at the specific frequency where imaginary component is zero, which corresponds to the point where the curve intercepts X axis (Figure 3).

Figure 4 shows typical temperature-dependent conductivity data for electrolytes formed by dissolving lithium bis(trifluoromethane sulfonyl)imide (LiTFSI) in polyethylene glycol dimethyl ether (PEGDME-500, average $M_n \sim 500$) at various O/Li ratios. As expected for thermally activated transport, the conductivity increases with temperature over the entire O/Li ratio range. The physical properties of the electrolyte also change with the O/Li ratio. For example, electrolytes at high O/Li ratios are low viscosity liquids at room temperature while a sample with a O/Li ratio of 8 (45 wt% of LiTFSI) is very viscous. LiTFSI has a molecular weight as high as 287 g/mol, this means every 287 g of LiTFSI has 7 g of lithium, giving a lithium content of 2.4×10^{-2} g Li/ g LiTFSI. This number is used to convert O/Li ratio to the corresponding LiTFSI content (wt%) in each mixture, as show in Table 4.

O/Li Ratio	8	16	32	64	96	128	256
LiTFSI Content (wt%)	44.9	29.0	16.9	9.2	6.4	4.8	2.5

Table 4. Weight content of LiTFSI in LiTFSI/PEGDME-500 at various O/Li ratios (2.4×10^{-2} g Li/ g LiTFSI).

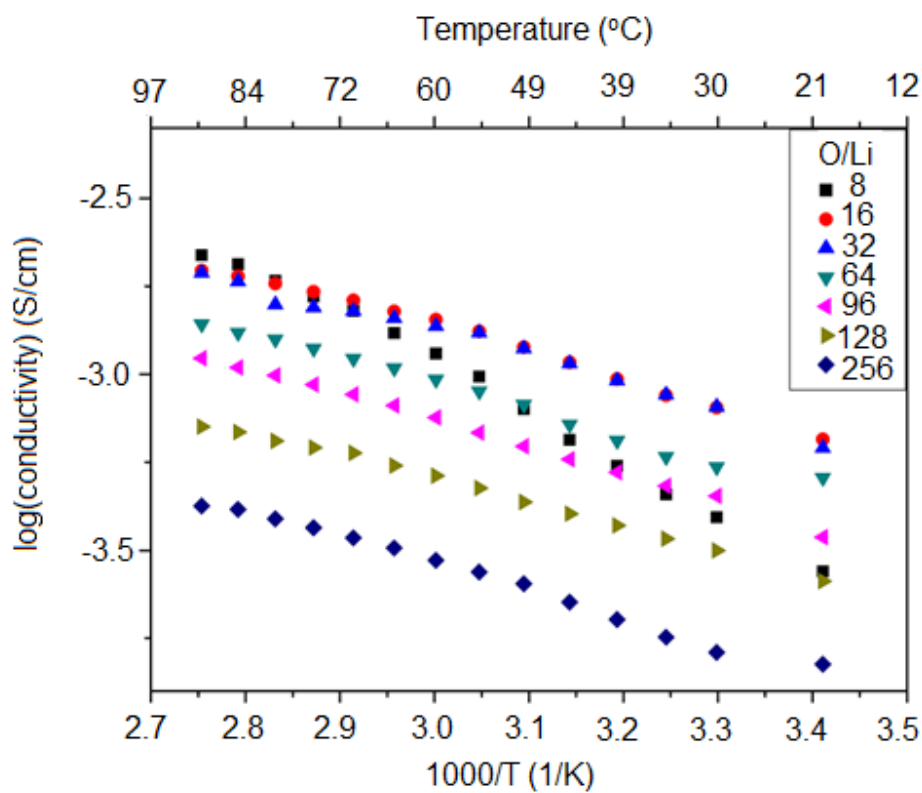


Figure 4. Temperature dependent conductivity for LiTFSI/PEGDME-500 electrolytes at various O/Li ratios.

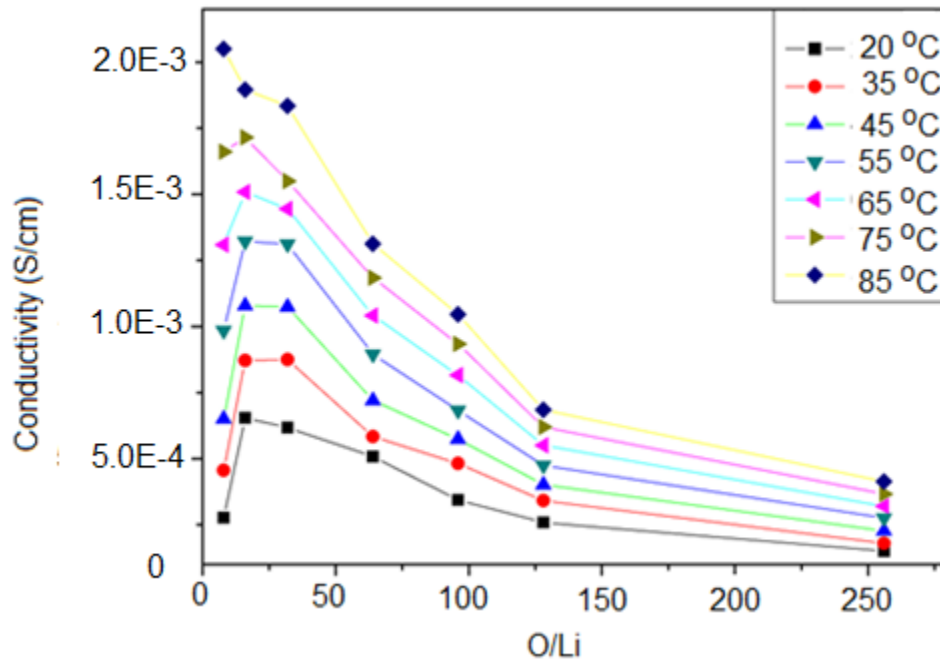


Figure 5. Conductivity as a function of the O/Li ratio for LiTFSI/PEGDME-500 electrolytes at various temperatures.

Figure 5 shows the same data set from Figure 4 plotted as conductivity as a function of the O/Li ratio. The data show that the conductivity increases with the lithium salt concentration, and then decreases after O/Li ratio of 8. These trends are often ascribed to decreased chain mobility at high salt concentrations and increased polymer T_g . (Attempts to prepare samples with an O/Li ratio of 4 (62 wt% LiTFSI) did not result in useful samples since the LiTFSI did not fully dissolve in the PEGDME-500 matrix.)

1.4. Lithium transference number

In a lithium ion battery, the electrolyte is comprised of a lithium salt dissolved in a solvent. As the battery is discharged, electrons flow from the anode to the

cathode through the external circuit, while inside the cell, lithium cations migrate from the anode to the cathode and intercalate into the cathode. Typical measurements of the Li^+ transference number (t_{Li^+}) in PEO-based electrolytes range from 0.2-0.4 (Table 5), which indicates the anion as the dominant species in Li^+ transport.

Lithium Salt	Polyether (or solvent system)	O/Li (concentration)	Temperature	t_+
LiClO_4	PEO1000	20:1	30 °C	^a 0.23
LiCF_3SO_3	PEO1000	24:1	30 °C	^a 0.21
LiBF_4	PEO500	20:1	70 °C	^b 0.32
LiPF_6	PC/EC/DMC (1:1:1)	1 M	Room Temperature	^b 0.38±0.04

^a data collected using Tubandt Technique

^b data are collected using galvanostatic polarization method

Table 5. Lithium transference numbers for typical lithium salts.

Determining accurate lithium transference values from the alternating current, direct current polarization, and Hittorf/Tubandt methods has been challenging. Recently, two methods were introduced, the DC polarization method developed by Bruce and Vincent,¹² and pulsed field gradient (PFG) measurements. The latter provides ion diffusion rates, which can differ from transference numbers obtained from the DC polarization method.

The DC polarization experiment, also called steady-state method, uses a

sample cell comprised of the electrolyte sandwiched by two lithium metal non-blocking electrodes. A potentiostat is used to apply a small DC polarization voltage (ΔV) across the sample, and the initial (I_0) and final steady-state (I_S) currents are determined. AC impedance spectroscopy is used to determine the electrolyte resistances before (R_0) and after (R_S) the potentiostatic measurements. The lithium cation transference number (t_{Li^+}) of the electrolyte samples is calculated from the following equation.

$$t_{Li^+} = \frac{I_S(\Delta V - I_0 R_0)}{I_0(\Delta V - I_S R_S)}$$

The significance of a low t_+ is polarization of the lithium ion cell during charging and discharging. Clustering of cations and anions forms a concentration gradient that limits the current during charge and discharge (Scheme 2). The resulting internal resistance generates heat during the charge and discharge process, limiting the power density of the battery and often affects the chemical stability of electrolyte. Thus, the effective voltage during discharge is V (cell voltage) - V_p (polarization voltage), and the voltage needed to charge the cell is $V + V_p$.

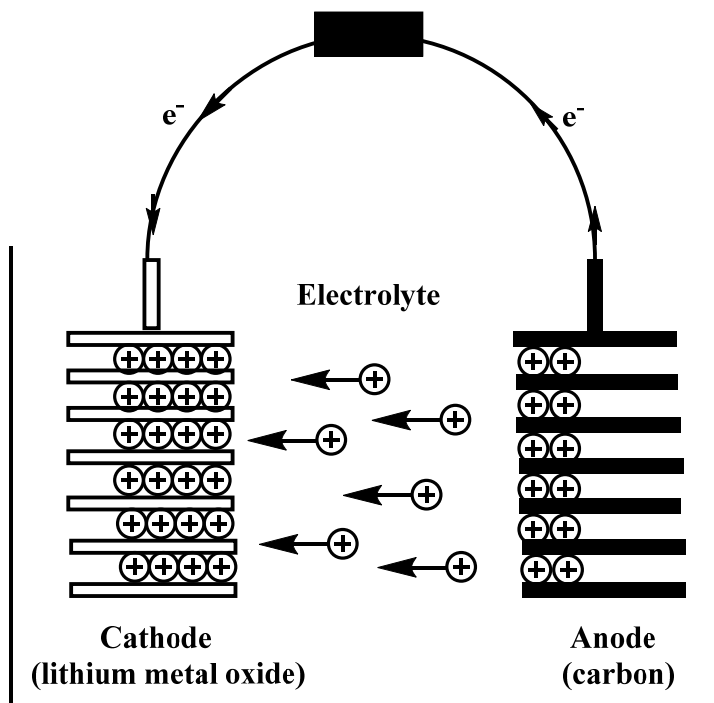
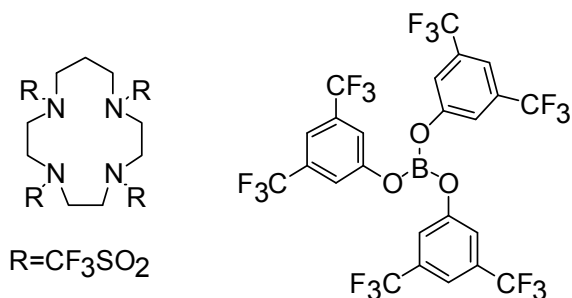


Figure 6. Polarization during discharge of a lithium ion battery.

Besides polarization, the conductivity of polymer lithium salt complexes tends to reach a maximum and then decrease as the lithium salt concentration increases. At high salt concentrations, triple or higher ionic aggregates form, decreasing the number of charge carriers, conductivity, and cell efficiency. Additives that preferentially interact with anions have been explored to increase the lithium ion transference number in electrolytes. Alternatively, the anions can be immobilized on polymers or on particle surfaces.

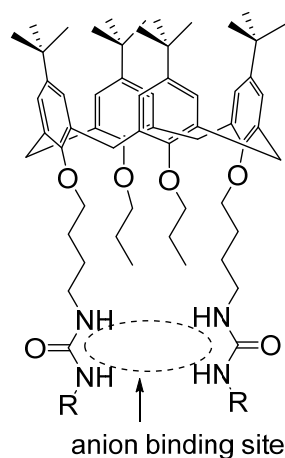
1.5. Electrolytes with high t_{Li^+} in literature

McBreen and coworkers synthesized anion receptors based on aza-ether^{13,14} and fluorinated boron compounds (Scheme 2).¹⁵ These compounds were used as additives in aprotic polar solvents, THF for aza-ether



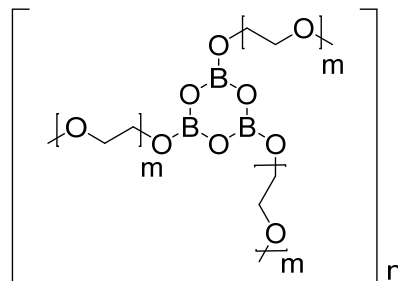
Scheme 2. Typical aza-ether and boron derivatives in McBreen's work.^{13, 14}

derivatives, 1,2-dimethoxyethane for boron derivatives. While the receptors successfully complexed bromide and chloride anions, the corresponding lithium salts (LiBr, LiCl) are not typically used in lithium ion batteries.



Scheme 3. A typical calixarene derivatives in Wiczorek's work.¹⁶

Wiczorek and coworkers synthesized calixarene^{16,17} and calixpyrrole^{18,19} derivatives for use as anion-binding additives in PEO-lithium salt electrolytes. The lithium transference number, measured by the steady-state technique, increased from 0.1 to 0.6, depending on the concentration of the additives and the temperature.



Scheme 4. Boroxine containing polymer in Mehta's work.²¹

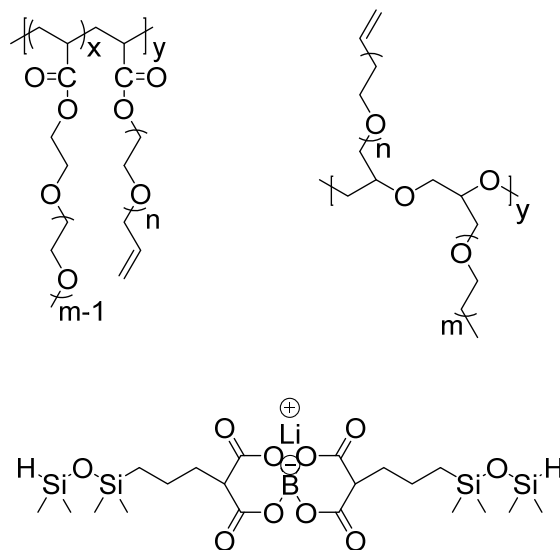
In conventional lithium salts, such as $\text{Li}(\text{CF}_3\text{SO}_2)_2\text{N}$, LiCF_3SO_3 , LiBF_4 , LiClO_4 , LiBr , LiCl , LiPF_6 , the anions are intrinsically Lewis bases. Mehta et al. constructed a PEO gel with boroxine rings as a cross-linker.^{20,21,22} The Lewis acidic boroxine rings interact with anions and suppress their mobility. Lithium transference numbers in these systems range from 0.6-0.9, compared to 0.2-0.3 for normal PEO-lithium salt systems. The increase in the lithium transference number in Mehta's system is high, considering the simplicity of its synthesis. The maximum room temperature conductivity was $\sim 10^{-5}$ S/cm.

Using the concept of trapping anions, Angell and co-workers synthesized "base-in-chain" and "acid-in-chain" polymers. Incorporating sulfonylimide groups into the polymer backbone gave a base-in-chain polymer. AlCl_3 was added to reduce the dissociation energy between the imide anion and lithium cation, resulting in a high ambient conductivity (1.6×10^{-4} S/cm). The conductivity was thought to be mainly cationic, but transference number measurements were not reported.²³ In addition, free AlCl_3 caused side reactions in the cells. For the acid-in-chain case, an open chain boron was incorporated into a PEO backbone.

A conventional lithium salt was added and the anion was trapped by the acidic boron. The properties of this system depended on the added lithium salt; for LiTFSI, the ambient conductivity was 7.6×10^{-5} S/cm.²⁴ The boron structure in the polymer also was converted to anionic sites by reaction with phenyllithium,²⁵ leaving Li^+ as the only mobile ion species and fulfilling the single-ion concept.

Scrosati promoted the use of composite polymer electrolytes, formed by adding ceramic powders to mixture of PEO and lithium salt.²⁶ It was claimed that the ceramic dispersion improved the interfacial stability between lithium metal and the polymer electrolyte,²⁷ and that the ionic conductivity and transference number were enhanced. However, Shriver and coworkers²⁸ studied lithium salt/PEO/SiO₂, Al₂O₃ nanoparticle systems, and their data showed that most important effect of the particles was a reduction of the PEO crystallinity, but there was no direct evidence for enhancement of conductivity in the amorphous phase.

Another way to get single cation conductors is to attach anions to polymers through covalent bonds, leaving the lithium cation as the only mobile ion. As long as all anions are tethered to the polymer, the lithium transference number should be unity.

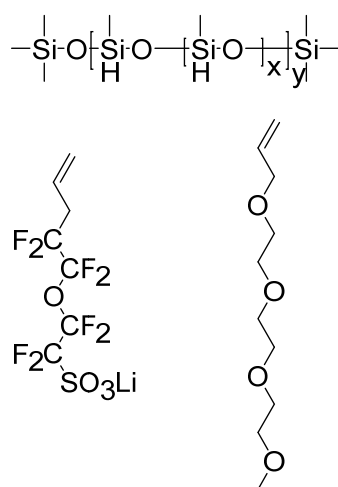


Scheme 5. Two prepolymer structures (top) and the boron cross-linker (bottom) used in Kerr's work.^{29,30,31}

Kerr et al. constructed two cross-linked networks that exhibited single ion conduction, where a lithium borate structure served as the lithium source and the cross-linker (Scheme 5). In one case, a polyacrylate/polymethacrylate backbone with a mixture of methoxy and allyl terminated PEO side chain structure was used. The highest ambient temperature conductivity was 3.5×10^{-7} S/cm and the single-ion conducting behavior was confirmed in a symmetrical lithium cell cycling test.²⁹ In another example, PEO and trimethylene oxide (TMO) chains were attached to a poly(epoxide ether) backbone.^{30,31} Conductivities were $\sim 10^{-6}$ S/cm, and Li/Li cell cycling tests showed no polarization.

Mayes and coworkers synthesized copolymers from lithium methacrylate (LMA) and polyethylene glycol methyl ether methacrylate (PEGMA).^{32,33} Both block copolymerization and random copolymerization were tried in their work. In

block copolymer, carboxylate anions phase separated from the ion-conducting PEGMA block, yielding room temperature conductivities of 10^{-7} S/cm; in random copolymer, ionic conductivities were one to two orders of magnitude lower. In another example from the same group, poly (dimethyl siloxane) methacrylate (PDMSMA) was incorporated into the copolymer,³⁴ When BF_3 was added to improve dissociation between the lithium and carboxylate ion, the room temperature conductivity was 7×10^{-6} S/cm at a O/Li ratio of 32. A test cell was constructed from a lithium anode, a vanadium oxide cathode, and the electrolyte. Lithium-ion intercalation into the cathode was hindered by the immobile anion in the electrolyte, causing an unexpectedly high polarization.^{35, 36}

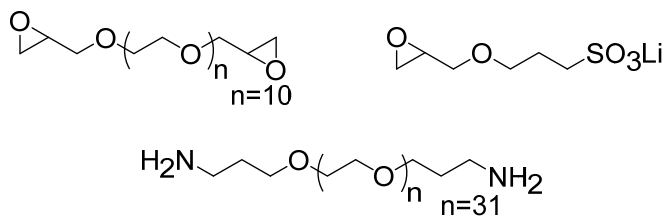


Scheme 6. Polysiloxane and side functionalities in Shriver's work.³⁹

Shriver and coworkers used Pt-catalyzed hydrosilylation reactions to attach trifluoromethylsulfonamide, perfluoroether sulfonate, and polyethylene glycol methyl ether side chains to polysiloxane backbones. Because of the low T_g of polysiloxanes, these comb polymers were expected to have a high conductivity.

Polysiloxanes with a mixture of polyethylene glycol methyl ether and trifluoromethylsulfonamide groups had a room temperature conductivity of 1.2×10^{-6} S/cm.^{37,38} Replacing the trifluoromethyl sulfonamide group with perfluoroether sulfonate slightly increased the conductivity to 2.5×10^{-6} S/cm with an O/Li ratio of 33:1.³⁹

Lithium siloxaluminatate polymers containing ethylene oxide side chains was synthesized by Rawsky and coworkers.⁴⁰ Conductivities of $\sim 10^{-5}$ S/cm were obtained, with a lithium transference number of 0.71.



Scheme 7. Monomers used in Endo's work.^{43,44}

Ohno and co-workers attached anion groups onto the chain ends of PEO oligomers. Ambient conductivities were in the range of 10^{-7} S/cm for carboxylate derivatives,⁴¹ 10^{-7} - 10^{-8} S/cm for benzenesulfonate derivatives, and 3×10^{-6} S/cm for sulfonamide derivatives.⁴² Endo and coworkers formed single ion conductors (Scheme 8) by using PEO diamines to ring-open epoxide monomers.^{43,44} The best ambient conductivity for these self-standing rubbery films was 3.4×10^{-5} S/cm, with the rest in the range of 10^{-6} S/cm.

A variety of particles have been tested for their ability to improve Li^+ transference numbers. Kurian et al. mixed lithium-exchanged montmorillonite clay

with poly [(oxyethylene)₈ methacrylate] and obtained low conductivities (10^{-8} S/cm).⁴⁵ Singhal et al. dispersed lithium-exchanged hectorite in a mixture of ethylene carbonate (EC) and polyethylene glycol dimethyl ether ($M_w = 250$), and reported ambient conductivities of $\sim 10^{-4}$ S/cm.⁴⁶ Riley combined lithium hectorite with carbonate solvents. The resulting mixture formed a physical gel with conductivities in the range of 10^{-3} - 10^{-4} S/cm and Li^+ transference numbers of 0.6-0.8.⁴⁷ To inhibit anion mobility, Fedkiw and coworkers attached sulfonate groups on silica nanoparticles and dispersed the particles in PEO oligomers.^{48,49}⁵⁰ While the Li^+ transference number was encouraging, the room temperature conductivity was $\sim 10^{-6}$ S/cm. Fedkiw and coworkers used free radical polymerization to modify the silica particles, which may have resulted in low polymer content and low lithium content.

Archer et al. grafted PEG chains to SiO_2 (8 and 18 nm) and TiO_2 nanoparticles (15 nm). LiTFSI was added to form a 1 M electrolyte in the organic phase. The conductivity was insensitive to the type of metal oxide or the nanoparticle size, but it increased with the molecular weight of the PEG chain. The highest room temperature conductivity was $\sim 10^{-4}$ S/cm with PEG chains with ranging from 595-725 g/mol. Most of the PEGs used in this work were liquids, but after grafting, the particle surface was an amorphous solid.⁵¹

With the development of controlled radical polymerization methods, such as atom transfer radical polymerization (ATRP), reversible addition-fragmentation

chain transfer polymerization (RAFT), and nitroxide mediated polymerization (NMP), surface polymerization became a practical method for modifying surfaces. A broad range of organic/inorganic hybrid materials have been synthesized that are comprised of an inorganic core with a polymer shell. Once initiators are bound to the surfaces of an inorganic particles, a dense layer polymer film can grow from the surface, termed the “grafting from” approach.⁵²⁻⁵⁵ Most work in this area have used ATRP, but other controlled radical methods also can be used.

In order to improve proton conductivity in membranes, Yameen and coworkers coated the membrane pores with ATRP initiators, and then grew brushes from a mixture of oligo(ethylene glycol) methacrylate and 2-sulfoethyl methacrylate. Including the hygroscopic oligo(ethylene glycol) chains was claimed to cause a 10^5 increase of the proton conductivity.⁵⁶

A previous group member, Dr. Yuan grafted sulfonic acid containing polymer on 7 nm silica particles, she mixed the hybrid particles with polyvinylidene fluoride (PVDF) to form composite proton exchange membranes (PEM). This composite PEM with 40 and 50 wt% particle contents gave proton conductivities comparable or even higher than Nafion 117.⁵⁷

We investigated several nanoparticle systems where lithium counterions are immobilized on polymers, the polymers are further attached to nanoparticles. Electrolytes were prepared from the purified particles and low-molecular weight (~500 g/mol) polyethylene glycol dimethyl ether (PEG -DME500). Initiators were

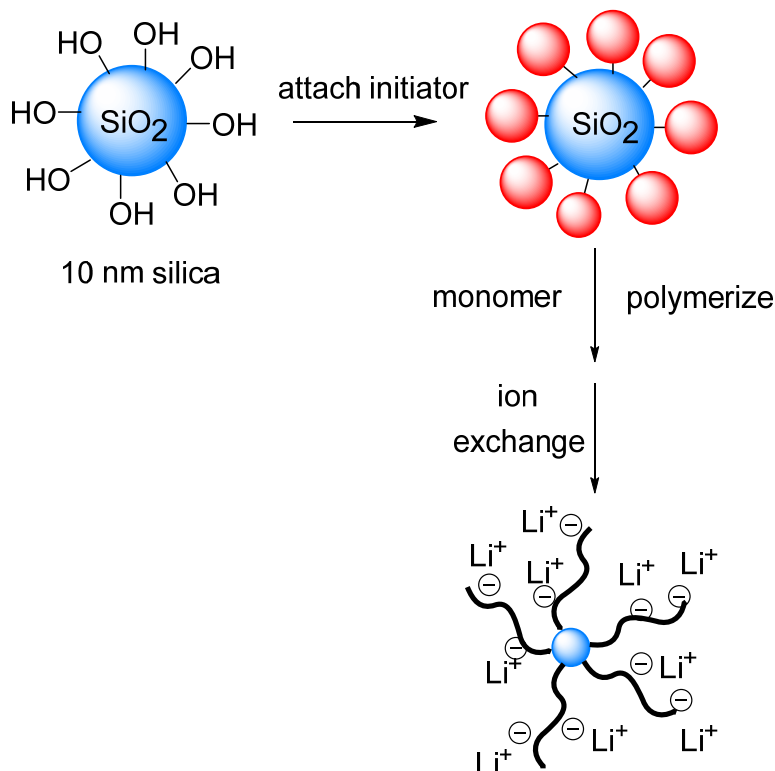
attached to 10 nm silica nanoparticles, and using Atom Transfer Radical Polymerization (ATRP), a controlled method useful for growing polymers from the surfaces. Four different structures were used in this work, aiming to get a high lithium conductivity.

2. Results and Discussion

Anchoring anions on nanoparticles should increase the Li^+ transference number to near unity since anions bound to particles have reduced mobilities. Previously, we and others examined anions attached to the surface of fumed silica (AEROSIL 200 from Degussa, surface area of $200 \text{ m}^2/\text{g}$) and spherical silicas.^{58,59} Apparently, decorating particle surfaces with a monolayer of anions provides too few anions to support high conductivity in a bulk electrolyte (O:Li ratio = 120). One strategy for increasing conductivity is to increase the available surface area by using smaller nanoparticles or higher surface-area particles (roughened). Commercially available particles have surface areas of $302 \text{ m}^2/\text{g}$ (for Snowtex-S of Nissan Chemical). Assuming all of the surface area is accessible, the O/Li ratios would improve to ~ 80 .

An alternative approach to increasing anion concentrations is to move from monolayer coverage of particles to polyelectrolytes anchored to particle surface (Scheme 9). In principle, the carrier concentration can be increase arbitrarily and approach the carrier concentration of the bulk polyelectrolyte. This can be accomplished by growing polymers from particle surfaces, especially by

controlled polymerization methods, such as ATRP. The research described in this dissertation focuses on nanoparticle systems where lithium counterions are immobilized on polyelectrolytes grown from nanoparticles.



Scheme 8. Synthetic approach to polyelectrolyte-decorated nanoparticles.

The synthetic route to polyelectrolyte-decorated nanoparticles is shown in Scheme 8. The nanoparticles were Snowtex-S (Nissan Chemical), a colloidal silica dispersed in pH 9-10 water, with an average particle size of 7-10 nm. The TEM image of the as-received particles is shown in Figure 7. Each step in the synthesis was confirmed by IR spectroscopy. As shown in Figure 8, the IR spectrum of Snowtex-S particles shows the characteristic bands 800-900

cm⁻¹ associated with to the Si-OH, and a broad absorption band at 1150 cm⁻¹.

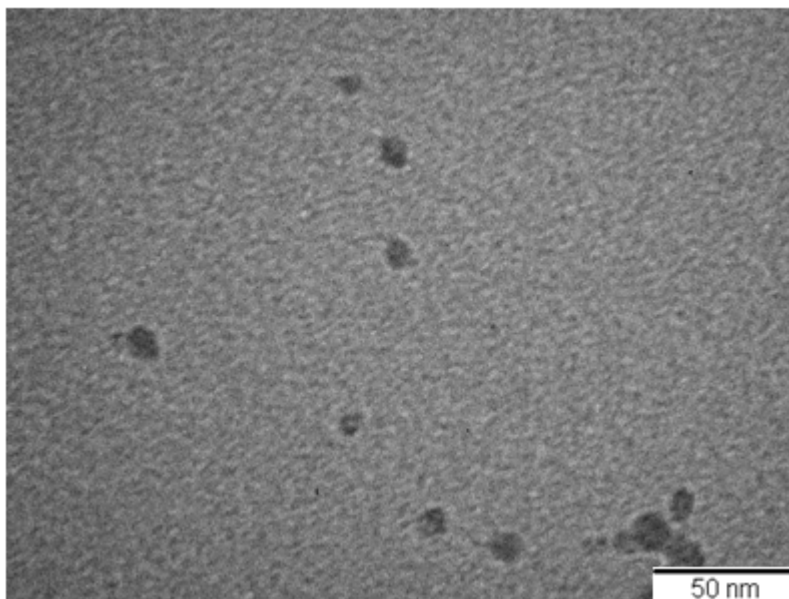


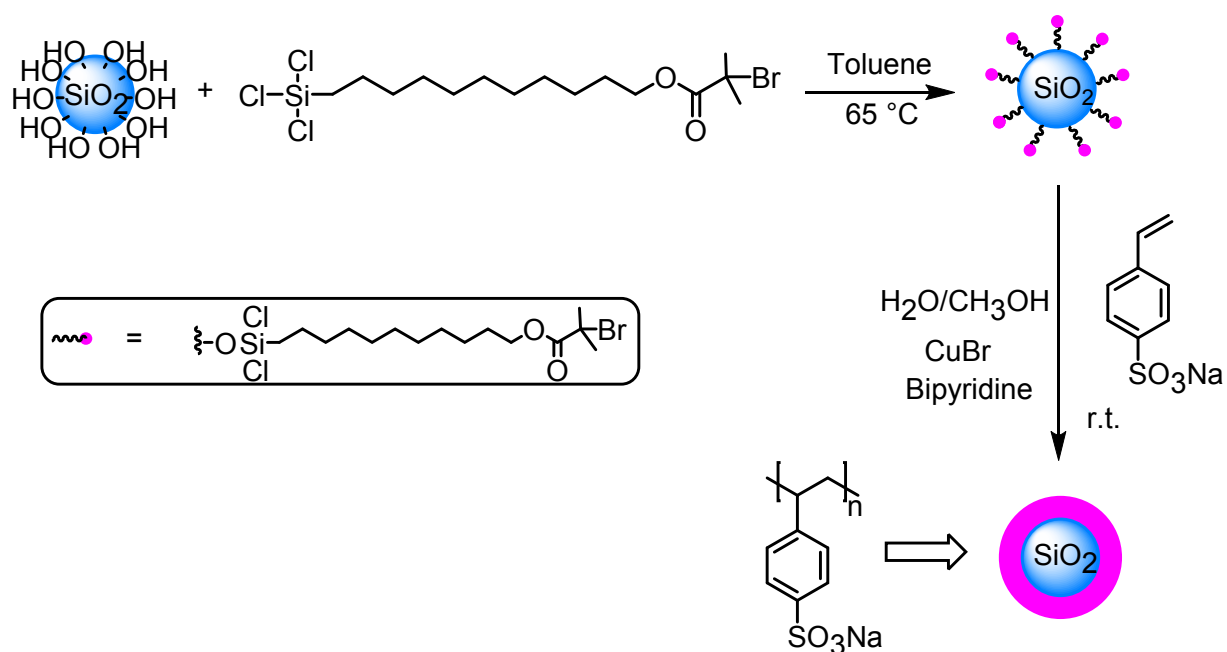
Figure 7. TEM image of Snotex-S silica nanoparticle (samples were dispersed in water and dropped on copper grid, and dried before taking TEM).

In addition, C-H stretching bands at 2800-3000 cm⁻¹ associated with cetyltrimethylammonium bromide⁴² (CTAB), a surfactant added to stabilize the nanoparticles in non-aqueous solvents. After anchoring the ATRP initiator (11-(2-bromo-2-methyl)propionyloxy)undecyltrichlorosilane to the nanoparticle surface, a new band appeared at 1700 cm⁻¹ (C=O) as the initiator displaced the CTAB.

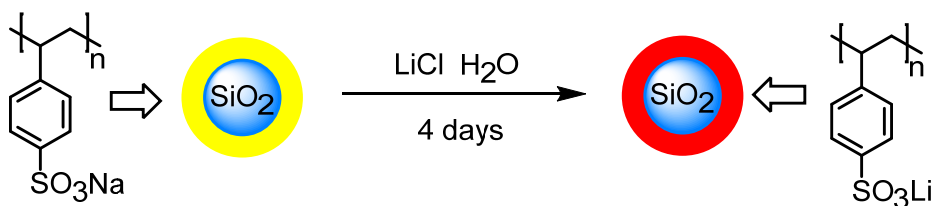
2.1. Particles modified with lithium 4-styrenesulfonate

For the preparation of poly(lithium styrene sulfonate) brushes on nanoparticles, we followed the procedure of Yuan.⁵² ATRP was used to grow poly(sodium styrene sulfonate) on particle surfaces at room temperature in a mixture of

methanol and water (1:3), using $\text{Cu}(\text{bpy})_2$ as the catalyst. After polymerization, the particles were purified by washing with mili-Q water (50 mL x 10). The poly(sodium styrene sulfonate) modified particles were converted to the corresponding Li^+ salt by treating the particles with aqueous LiCl (100 equivalents) for four days at room temperature (Scheme 10). The particles were recovered by centrifugation, washed 10 times with Mili-Q water, and dried at 90 °C under vacuum overnight.



Scheme 9. Immobilization of initiator on silica particle and the following surface ATRP with sodium 4-styrenesulfonate (SSNa).



Scheme 10. Lithiation of silica particle grafted by poly(sodium 4-styrenesulfonate) (Si-PSSNa).

The IR spectrum of the poly(lithium styrene sulfonate) brushes showed strong bands associated with the sulfonate group (S=O stretching, $980\text{-}1225\text{ cm}^{-1}$, S-O stretching, $690\text{-}870\text{ cm}^{-1}$). Overtones and combination bands at $1800\text{-}2000\text{ cm}^{-1}$ and the out-of-plane CH bending at 817 cm^{-1} are characteristic of the para-substituted benzene rings, expected for the styrene moiety, confirming the successful growth of the polymer from the surface.

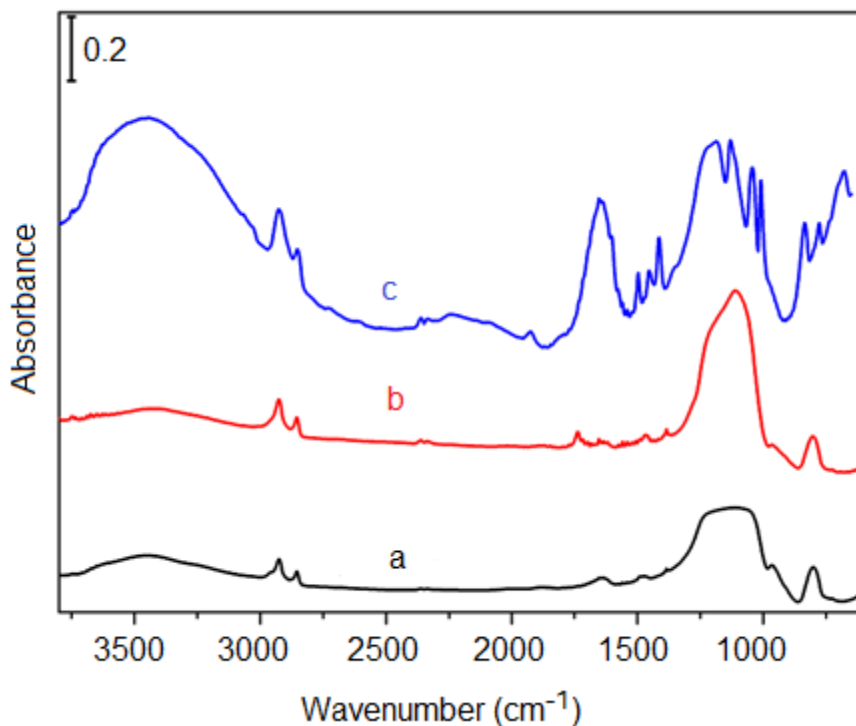


Figure 8. FTIR spectra of (a) Snowtex-S silica particles; (b) Si-Initiator, initiator

grafted silica particles; (c) Si-PSSLi, poly (lithium 4-styrene sulfonate) grafted silica particles.

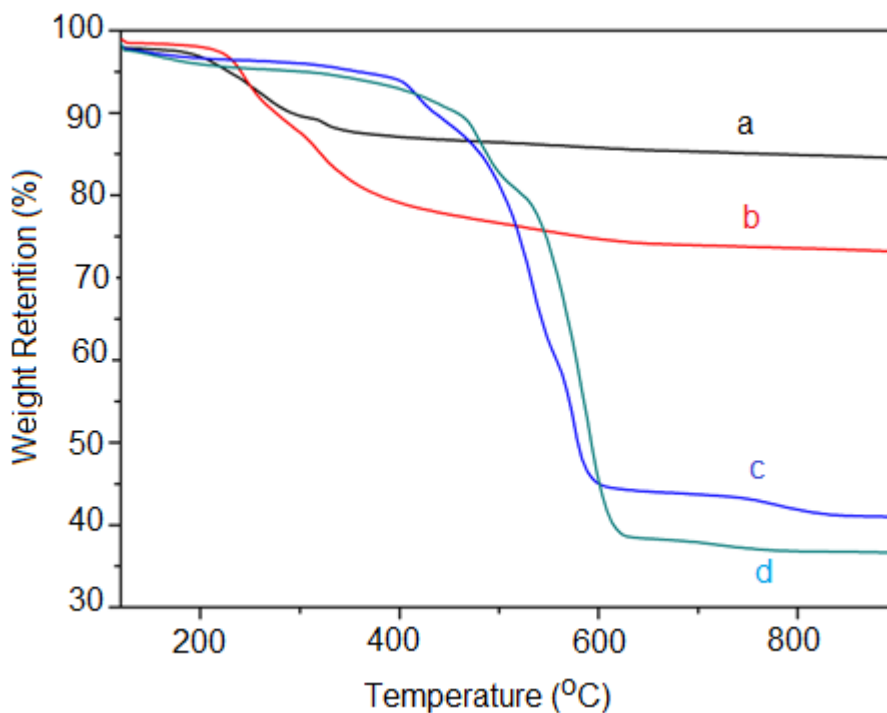
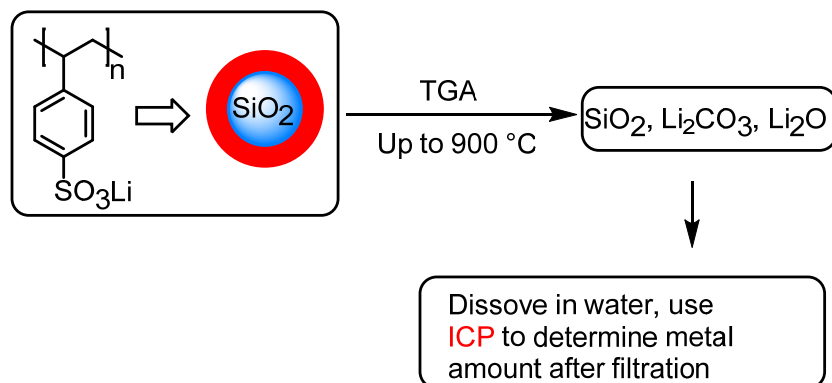


Figure 9. Thermogravimetric Analysis (TGA) curves of (a) Snowtex-S bare particles; (b) initiator grafted silica particles; (c) Poly(sodium 4-styrenesulfonate) grafted silica particles; (d) Poly(lithium 4-styrenesulfonate) grafted silica particles.

Figure 9 shows the Thermogravimetric Analysis (TGA) data of sulfonate styrene monomer system up to 900 °C in air. Under oxygen at this high temperature, all the organic component were lost, and the weight loss here gave information about organic content on silica particle surface. All the particle samples were dried at 90 °C under vacuum line before characterization. The silica particles had a weight loss of 15 wt% at 800 °C. The mass loss includes the CTAB surfactant, adsorbed

water, and water formed by condensation of surface bound silanols. According to the information provided by Nissan Chemical Co., the surface area of Snowtex-S sample is $302 \text{ m}^2/\text{g}$, cross section of the ammonium bromide group on CTAB is 0.8 nm^2 . On one extreme case, to estimate the minimum residual CTAB on particle surface, all the CTAB would be washed out, which give a 0 wt% weight loss; on the other extreme case, to estimate the maximum residual CTAB on particle surface, there would be one whole layer of CTAB molecule on the particle surface, based on the surface area of the particle and cross section of the ammonium group, it gives 16.5 wt% weight loss. This TGA value of 15 wt% fall in between 0 ~ 16.5 wt%. For calculation of the initiator-modified particles, assuming $0.6 \text{ nm}^2/\text{initiator chain}$, theoretical weight loss of the organic component should be around 15.1 wt%.⁶⁰ Initiator grafted silica particles showed weight loss of 27%, the residual water might add up the weight loss of the sample. The high weight loss of sample c (64%) and d (72%) proved that surface polymerization was successfully done. For the TGA data of Na and Li polyelectrolytes, the residue at $900 \text{ }^\circ\text{C}$ should be comprised of the silica particle and Li and Na oxides or salts. As expected, PSSLi had the largest weight loss, as lithium has the lower atomic weight.



Scheme 11. Quantitative determination of metal content.

Quantitative analysis of the metal content in the TGA residue by Inductive Coupled Plasma (ICP) optical emission spectrometry provides an estimate of the number of anions bound to the nanoparticles. The lithium should be in the form of Li_2O or Li_2CO_3 ; both are water soluble. For the ICP analysis, the TGA residue was stirred in Milli-Q water for 12 h, and filtered prior to the analysis. ICP analysis of the TGA residue from a 6.6 mg Si-PSSLi sample gave 0.16 mg lithium, which corresponds to 2.4×10^{-2} g Li/g sample. This means more than 95% of the Na was exchanged with Li, this relatively high lithium content enables us to get a high lithium content concentration in the electrolyte (as high as a O/Li ratio of 32:1).

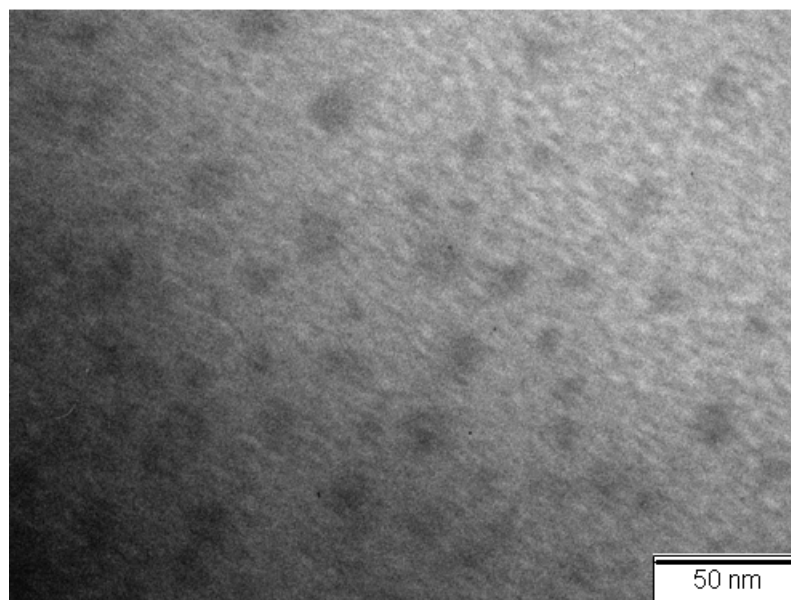


Figure 10. TEM image of Si-PSSLi (samples were dispersed in water and dropped on copper grid, dried before taking TEM).

Figure 10 shows TEM image of Si-PSSLi dispersed in water. The larger size of the polymer grafted particles is 15-20 nm, compared to the 7-10 nm of bare particles (Figure 7), consistent with successful growth of polymer from the particle surface. Electrolytes were prepared by mixing polymer grafted silica particles and poly(ethylene oxide) dimethyl ether oligomer ($M_w=500$) (PEGDME-500) at various O/Li ratios were made. Vigorous stirring for 24 hours resulted in homogeneous electrolytes.

O/Li ratio	32	64	96	128	192	256
Particle content (wt%)	17.2	9.4	6.5	4.9	3.3	2.5

Table 6. Particle weight content for electrolytes prepared from Si-PSSLi (2.4×10^{-2} g Li/g nanoparticles) dispersed in PEGDME-500.

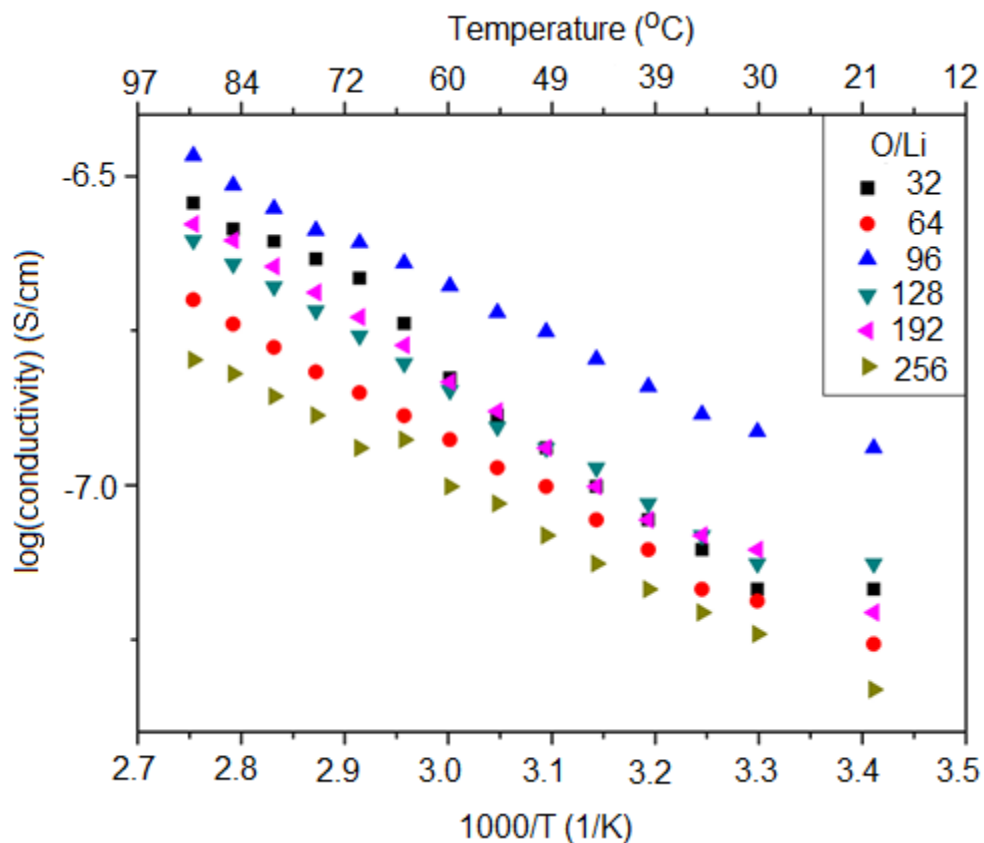


Figure 11. Temperature dependent conductivity for Si-PSSLi/PEGDME-500 at various O/Li ratios.

Figure 11 shows the temperature-dependent conductivity measured by impedance spectroscopy for electrolytes with different O/Li ratios. As the temperature increased, the conductivity increased, as expected for increased chain mobility for the PEGDME-500 host. The data are roughly linear, consistent with thermally activated transport and the VTF equation. The conductivity increased with decreased O/Li ratios (more carriers), but at the lowest ratios (highest particle content), 32, the conductivity decreased. The trends are more clear in Figure 12, where the room temperature conductivity is plotted as a

function of the O/Li ratio. Similar trends are seen in salt/PEO electrolytes (see Figure 5), which are usually interpreted as the formation of less mobile ionic aggregates or an increase in the T_g of the electrolyte. Here the anions are tethered to the polymer chains and the effects occur at higher O:Li ratios, suggesting that either an increase in the electrolyte T_g or a decline in the volume fraction of the conductive phase is responsible. Overall, the room temperature conductivity of the electrolytes is around 1×10^{-7} S/cm.

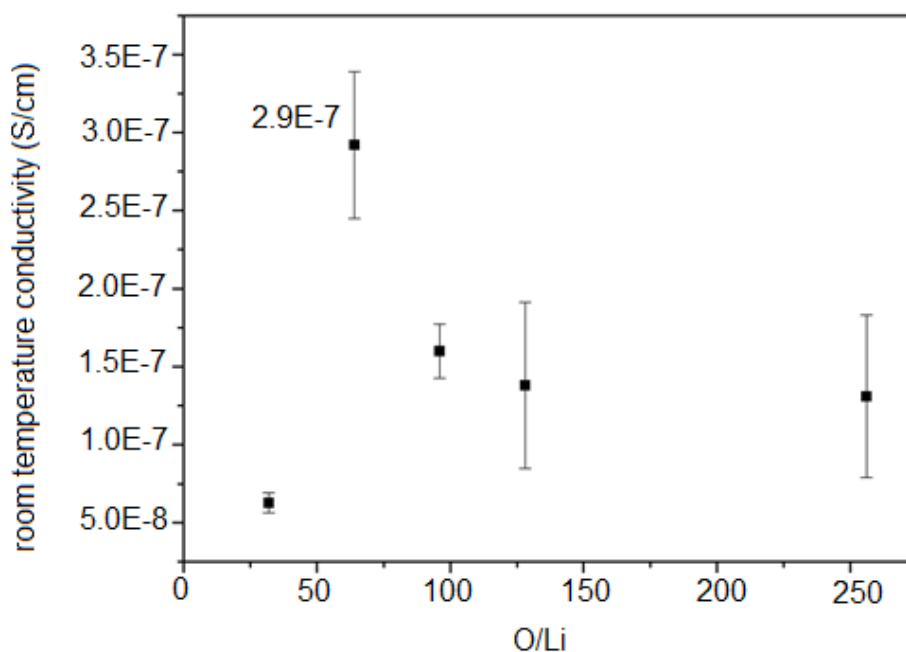
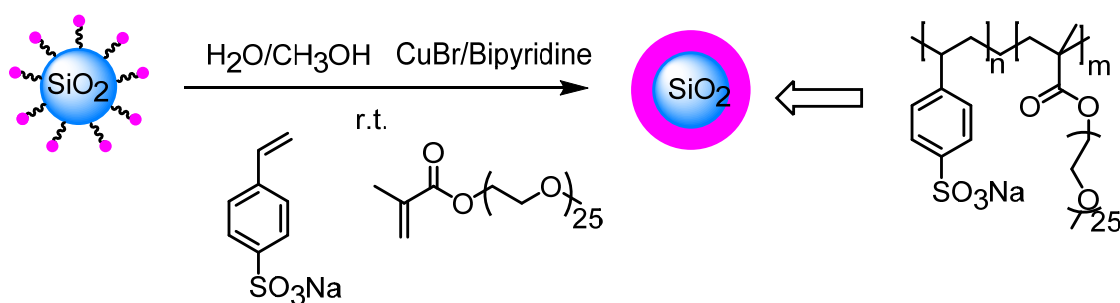


Figure 12. Room temperature conductivity vs. O/Li ratio for Si-PSSLi/PEGDME-500 electrolytes.

2.2. Particles modified with lithium 4-styrenesulfonate and PEGMA

We reasoned that the ion mobility may be hindered within the dense layer of lithium ions and aryl sulfonates coating the nanoparticles. To test that hypothesis

and hopefully increase the conductivity, we copolymerized PEGMA ($M_n=1100$) with sodium 4-styrenesulfonate from the particle surface. Copolymerization of PEGMA with sodium 4-styrenesulfonate would introduce PEG chains on the particles that might facilitate transport of lithium ion. In addition, adding PEG chains to the particles might improve the interface between the particles and the PEGDME-500 host.



Scheme 12. Copolymerization of SSNa and PEGMA monomers on silica particle.

The conditions for the surface-initiated copolymerization and workup procedure were similar to those used for the homopolymerization of sodium 4-styrenesulfonate (Scheme 12). The mole ratio of sodium 4-styrenesulfonate to PEGMA monomers was 3:1, which corresponds to a polymer layer with an O/Li ratio of 8:1 (two oxygen atoms of the ester group not included).

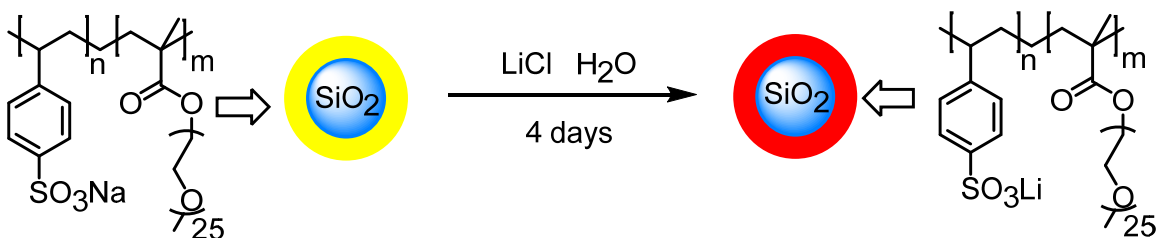
Since TGA was performed up to 900 °C, all the organic content would contribute to the weight loss, which provided information about amount of both monomers; ICP gave information about sodium content, which was only from the PSSNa structure. Combining TGA and ICP data (Scheme 13) gave ratio of this two monomers on particle surface, which was very close to the targeted monomer

ratio (3.45:1).

$$\frac{\text{SSNa content}}{\text{SSNa and PEGMA}} = \text{percent of SSNa on particle surface}$$

Na ICP (points to SSNa content)
Weight loss from TGA (points to SSNa and PEGMA)

Scheme 13. Characterization for the copolymer content in Si-PSSNa-PEGMA.



Scheme 14. Lithiation of Si-PSSNa-PEGMA.

Lithiation of this copolymer grafted particles was similar as previous. Excess of lithium chloride aqueous solution was used to change it to lithium electrolyte (Scheme 14). ICP data showed that 87.6% sodium content was converted to lithium, and lithium content was 1.6×10^{-2} g Li/g sample. Compared to Si-PSSLi sample, lithium content in this copolymer version was relatively lower, more particles need to be mixed to get the same O/Li ratio.

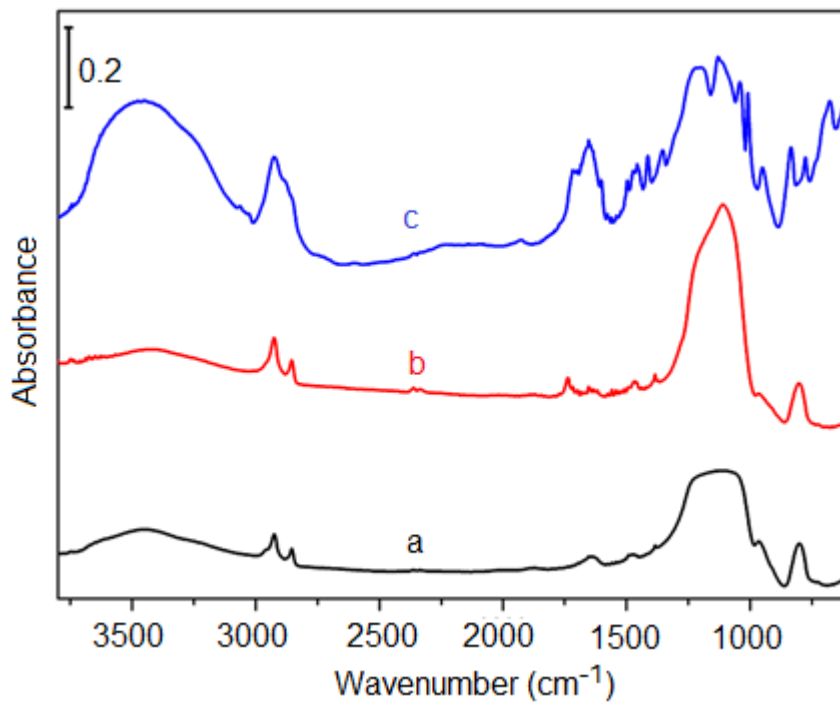


Figure 13. FTIR spectra of (a) Snowtex-S nanoparticles; (b) initiator grafted silica particles; (c) Co-poly(4-styrenesulfonate)-PEGMA grafted silica particles.

Compared to initiator grafted silica particles from FTIR spectra (Figure 13), the multiple bands at 980-1225 cm⁻¹ from S=O stretching and peaks at 690-870 cm⁻¹ from S-O indicate that polymer was successfully grown onto the particle surface.

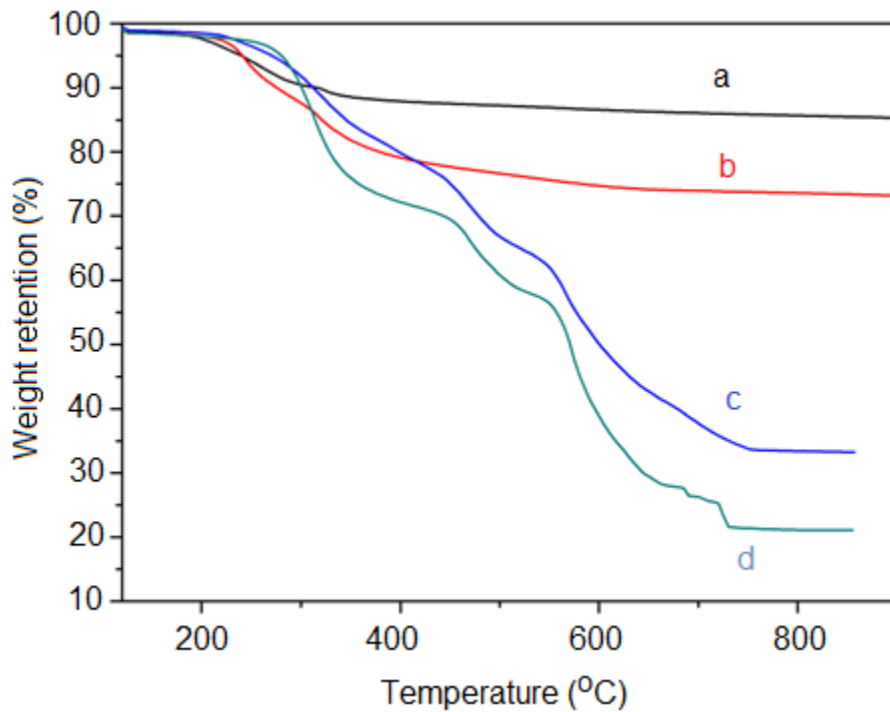


Figure 14. TGA curves of (a) Snowtex-S bare particles; (b) initiator grafted silica particles; (c) Co-Poly(sodium 4-styrenesulfonate)-PEGMA grafted silica particles; (d) Co-Poly(lithium 4-styrenesulfonate)-PEGMA grafted silica particles.

Figure 14 shows TGA curves of copolymer grafted silica particles. The high weight loss of sample c (68%) and d (82%) proved that surface polymerization was successfully achieved. The relative bigger weight loss compared to pure sulfonate monomer grafted system was due to the large side chain structure of PEGMA repeating unit.

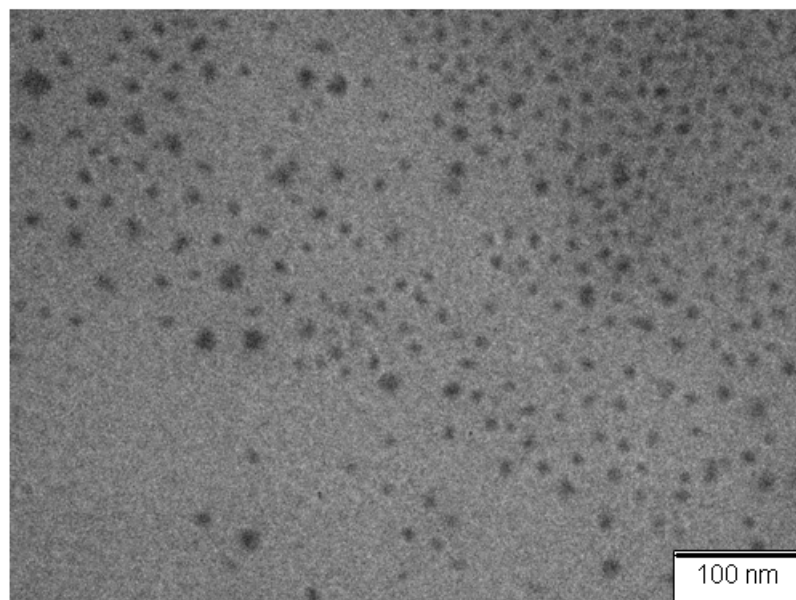


Figure 15. TEM image of Si-PSSLi-PEGMA (samples were dispersed in water and dropped on copper grid, dried before taking TEM).

Figure 15 shows TEM image of Si-PSSLi-PEGMA. The average size of the polymer grafted particles increased to 15 nm. The particles were mixed with PEGDME-500 to measure the conductivity at different O/Li ratios.

O/Li ratio	32	64	128	192	256
Particle content (wt%)	24.2	13.7	7.4	5.0	3.8

Table 7. Particle weight fraction for Si-PSSLi-PEGMA (1.56×10^{-2} g Li/g sample) dispersed in PEGDME-500.

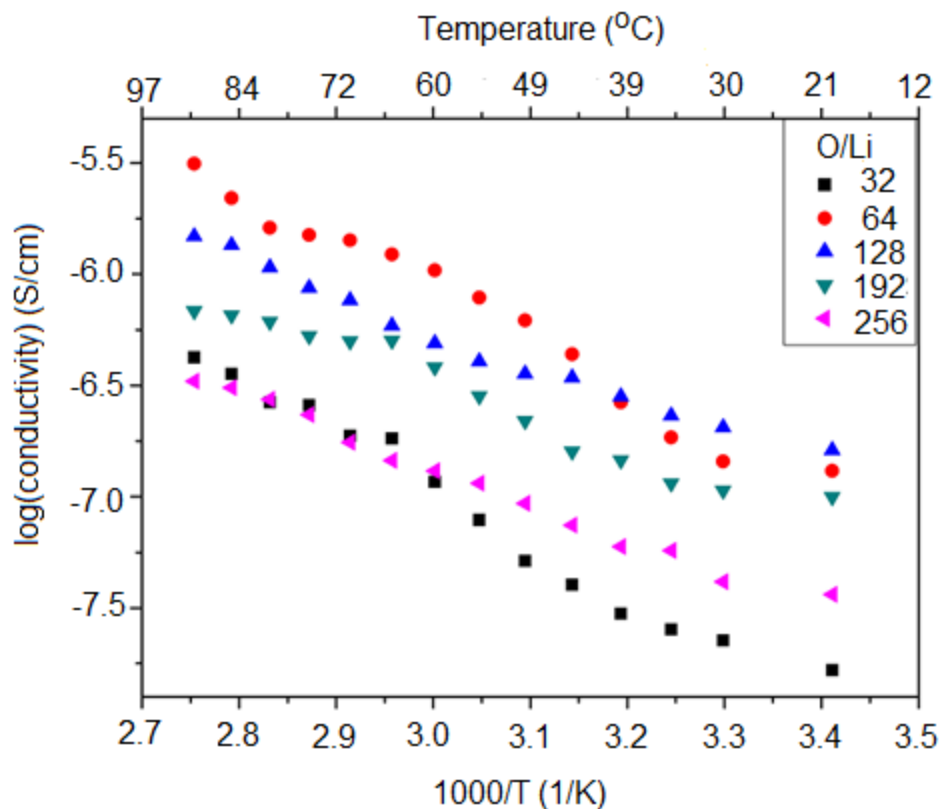


Figure 16. Temperature dependent conductivity of Si-PSSLi-PEGMA/PEGDME-500 at various O/Li ratios.

Figure 16 showed that for all samples at different O/Li ratio, conductivity increases with increase of the temperature. However, shapes of curves for different samples seem quite “noisy” for this system here.

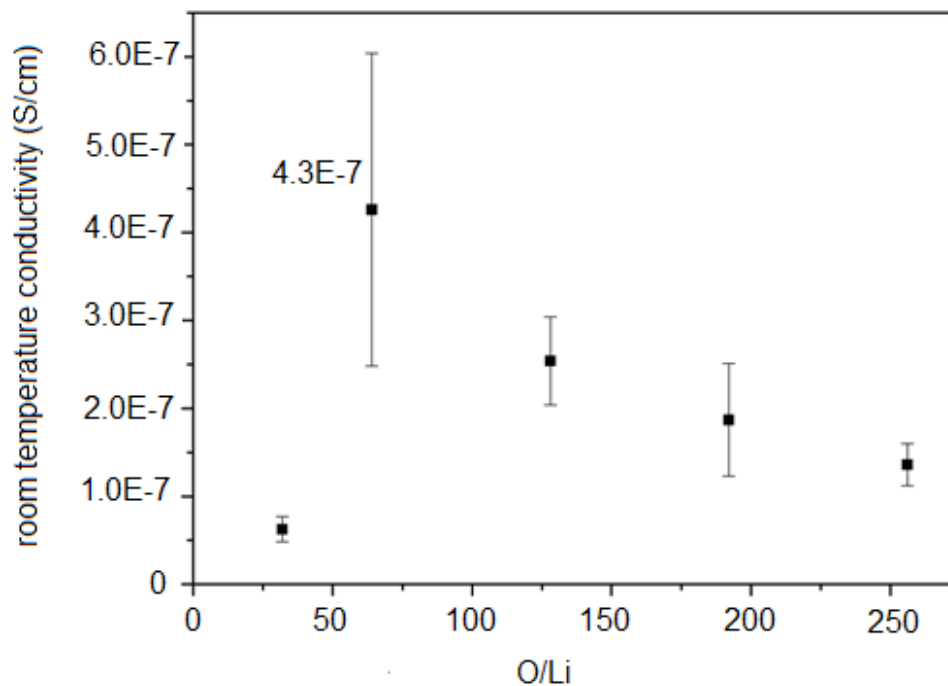


Figure 17. Room temperature conductivity VS. O/Li ratio for Si-PSSLi-PEGMA /PEGDME-500.

Room temperature conductivity reached a peak value of 4.3×10^{-7} S/cm at O/Li of 64 (Figure 17). Further increase of the particle content only resulted in decrease of the conductivity. Compared to the homopolymer modified particles Si-PSSLi, which has a peak value of 2.9×10^{-7} S/cm, conductivity of copolymer modified particles is relatively increased.

2.3. LiTFSI analogue polymer modified particles

Transference number and conductivity are the most important parameters for electrolyte material in lithium ion battery. In our study, the anion group was anchored onto the polymer backbone; to further immobilize the anion, the polyelectrolyte was anchored on surface of silica nanoparticles. This architecture

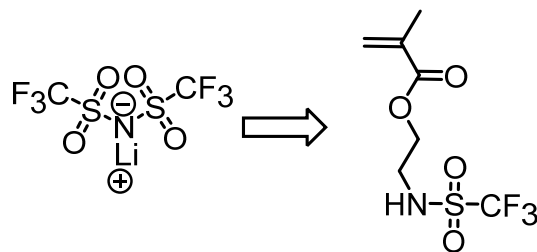
could ensure that most of the ionic conductivity was contributed from lithium cation. In this case, how to improve conductivity became our major concern.

According to the equation

$$\sigma(T)=n(\text{number of carriers}) * q(\text{charge of the carrier}) * \mu(\text{mobility})$$

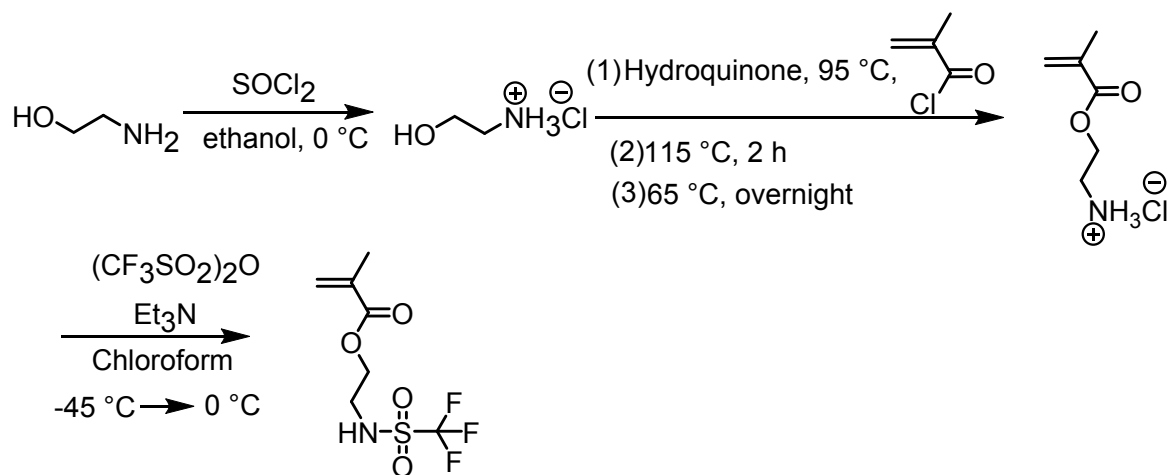
At a specific temperature, ionic conductivity is directly related to number of carriers, charge of the carrier and mobility of the carrier. We used PEGDME-500 oligomer as a model compound to study the properties of this architecture, this oligomer dominated mobility of the lithium cation, which is a factor we could not change; charge of lithium cation is $1.6 * e^{-19}$ Coulombic. We decided to focus on the first factor and try to increase number of carriers. In most of the cases, cation and anion formed compact ion pair, this hindered lithium cation mobility. Ue and coworkers'⁶¹ study showed dissociation degree of common lithium salt followed this order: $\text{Li}[\text{N}(\text{SO}_2\text{CF}_3)_2]$, $\text{LiAsF}_6 > \text{LiPF}_6 > \text{LiClO}_4 > \text{LiBF}_4 > \text{LiC}_4\text{F}_9\text{SO}_3 > \text{LiCF}_3\text{SO}_3$.

Because lithium bis(trifluoromethanesulphonyl)imide (LiTFSI) is well known for good conductivity and high dissociation degree, we proposed a new monomer to mimic its structure (Scheme 15). The methacrylate part of this structure makes it easily radical polymerized; a mono-trifluoromethane sulfonyl structure was retained to ensure a good dissociation degree with lithium cation.



Scheme 15. Trifluoromethane sulfonic aminoethylmethacrylate (TFMA) monomer inspired by LiTFSI structure.

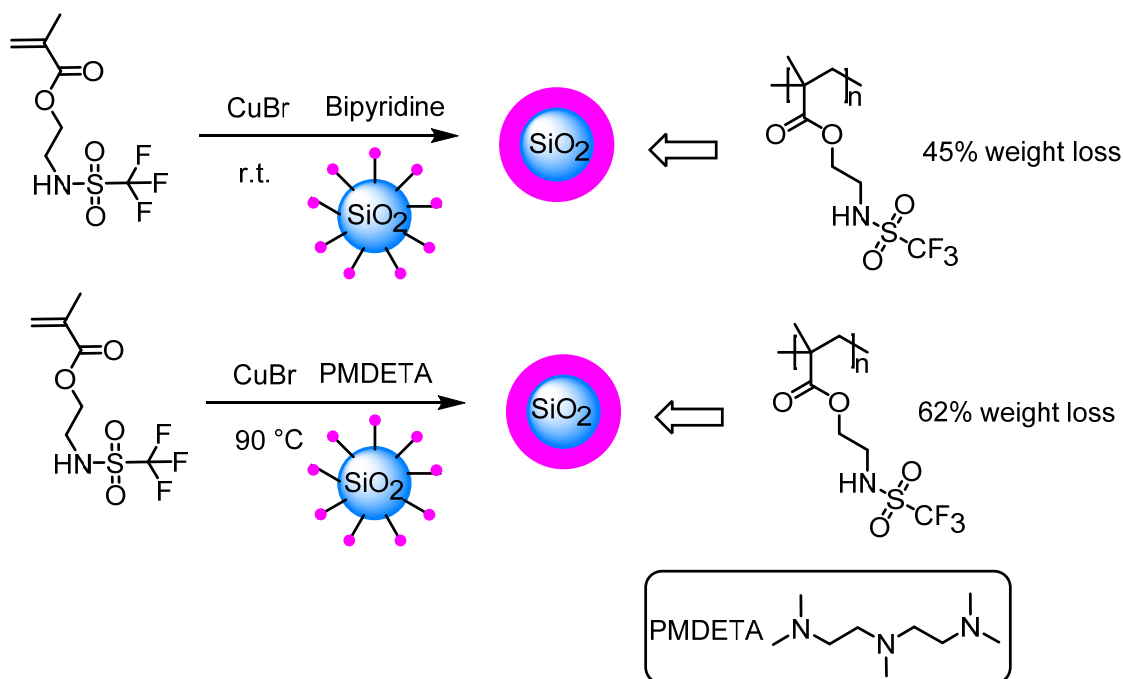
Once polymerized, post-modification with *n*-butyl lithium gave a lithium electrolyte. Admittedly, conductivity data of a mono-trifluoromethane sulfonyl structure would not be as good as its bis-version, but this was a necessary sacrifice to get a polymerizable structure.



Scheme 16. Synthesis of trifluoromethane sulfonic aminoethylmethacrylate (TFMA).

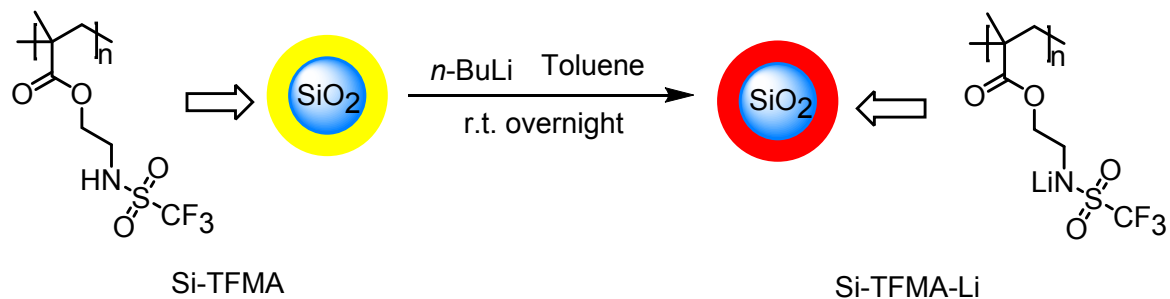
Ethanolamine was converted to amino salt to protect amine group. The following chemistry was done in the molten state without any solvent; hydroquinone was used as a radical scavenger. The methacrylate organic salt

intermediate was found only soluble in chloroform (Scheme 16). Trifluoromethane sulfonyl group was normally installed at -78°C , -45°C was chosen as reaction temperature to make sure the solvent was maintained as liquid state (m.p. of Chloroform -63°C).



Scheme 17. ATRP of trifluoromethane sulfonic aminoethylmethacrylate (TFMA) on silica particles.

Surface ATRP on silica particle using bipyridine as ligand at r.t. gave 45% polymer content. To get a thicker polymer layer, N, N, N', N', N''-Pentamethyldi-ethylenetriamine (PMDETA) was used as ligand, reaction temperature was increased to 90°C . As a result, product with 62% polymer content was obtained (Scheme 17).



Scheme 18. Lithiation of Si-TFMA to Si-TFMA-Li.

Lithiation of Si-TFMA was done using *n*-butyl lithium in dry toluene (Scheme 18). Overnight reaction at room temperature gave lithiation efficiency of 78%, and the lithium content in Si-TFMA-Li was 2×10^{-2} g Li/g sample.

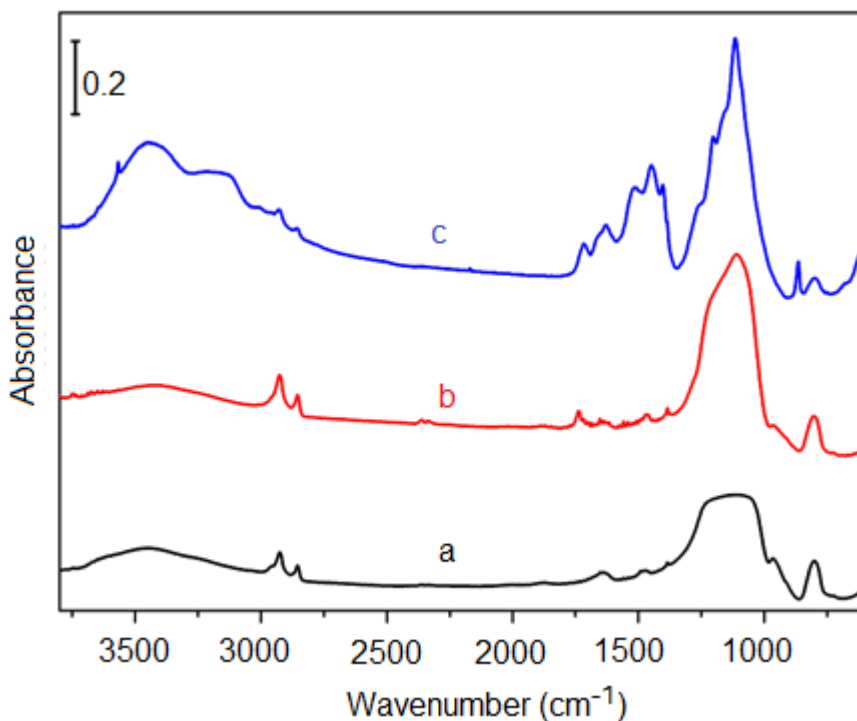


Figure 18. FTIR spectra of (a) Snowtex-S silica particles; (b) Si-Initiator, initiator grafted silica particles; (c) Si-TFMA-Li, lithiated poly(trifluoromethane sulfonic aminoethylmethacrylate) grafted silica particles.

Figure 18 shows FTIR spectra of the PTFMA grafted particles at different stages. Further development of the peak at 980-1300 cm^{-1} and split of the peak from FTIR spectra corresponds to S=O stretching, the sharp peak at 680-780 cm^{-1} was assigned to CF_3 stretching, both proved the polymer content on particle surface.

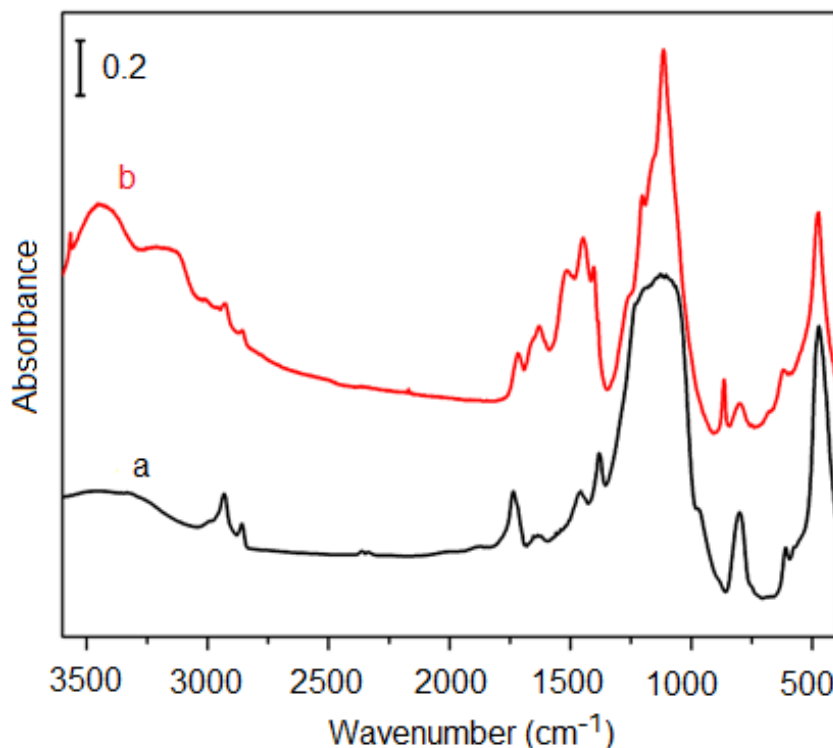


Figure 19. FTIR spectra of (a) Si-TFMA, poly(trifluoromethane sulfonic aminoethylmethacrylate) grafted silica particles; (b) Si-TFMA-Li, lithiated poly(trifluoromethane sulfonic aminoethylmethacrylate) grafted silica particles.

A potential problem with the lithiation of Si-TFMA was that the ester group might be susceptible to the strong base (*n*-BuLi). This reaction was characterized with ICP, which only gave the lithium content of the final product. However, lithium

cation could be on the imide group; or if the ester got hydrolyzed, lithium cation could also stay on the carboxylic group. To prove that final product Si-TFMA-Li maintained the original structure, FTIR spectra before and after lithiation was shown in Figure 18. If the polymer structure survived lithiation chemistry, ideally the two spectra would be the same, but there are subtle difference between the two spectra. As another tentative evidence, for the samples from different batches with the same weight loss in TGA, lithium content is repeatable after lithiation. However, none of these are conclusive.

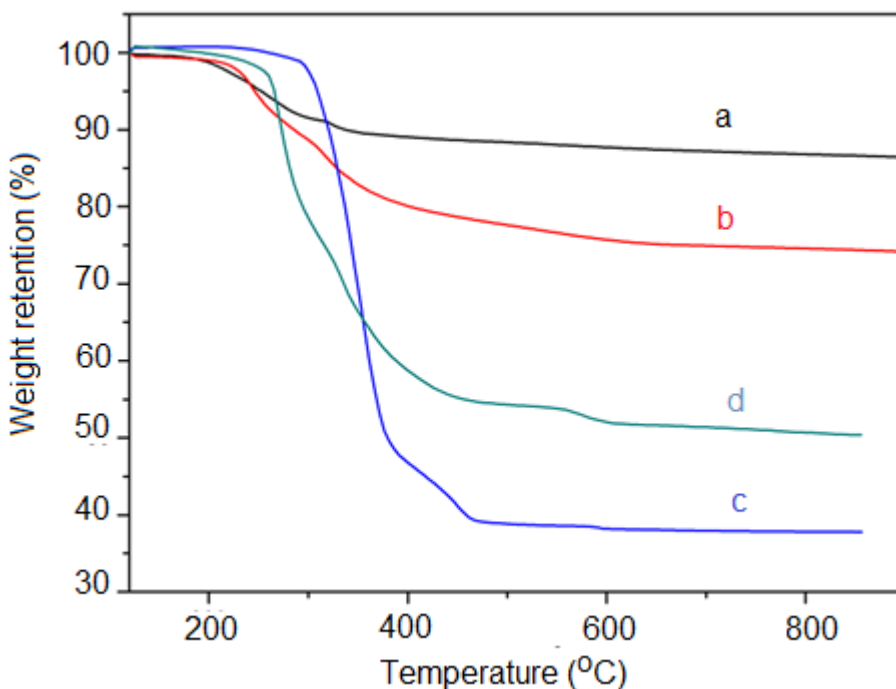


Figure 20. TGA curves of (a) Snowtex-S silica particles; (b) Si-Initiator, initiator grafted silica particles; (c) Si-TFMA, poly(trifluoromethane sulfonic aminoethylmethacrylate) grafted silica particles; (d) Si-TFMA-Li, lithiated poly(trifluoromethane sulfonic aminoethyl -methacrylate) grafted silica particles.

Figure 20 shows TGA curves of TFMA monomer grafted silica particles. The large weight loss of sample c (62%) and d (57%) proved that surface polymerization was successfully conducted. After lithiation, the lithium content was retained as oxide or salt, this made the weight loss of sample d smaller than sample c.

O/Li ratio	16	32	64	96	128
Partcile content (wt%)	33.2	19.9	11.1	7.7	5.8

Table 8. Particle weight content for electrolytes prepared from Si-TFMA-Li (2.0×10^{-2} g Li/g sample) dispersed in PEGDME-500

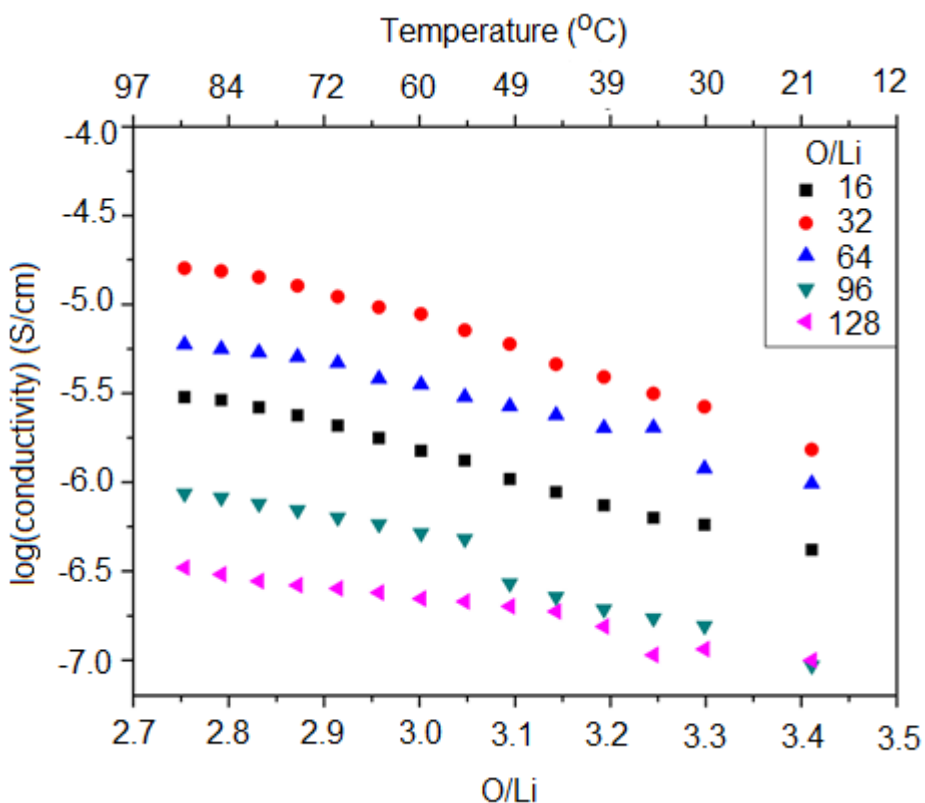


Figure 21. Temperature dependent conductivity of Si-TFMA-Li/PEGDME-500 at various O/Li ratios.

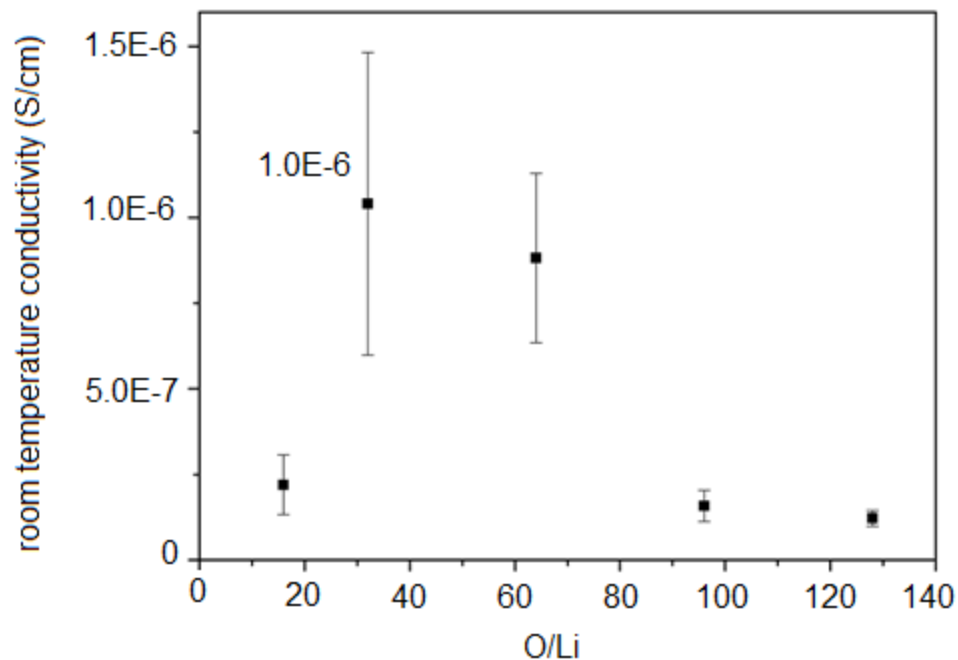
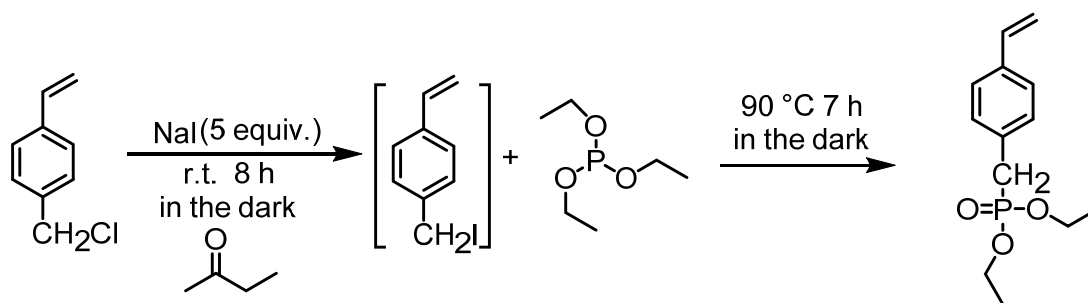


Figure 22. Room temperature conductivity vs. O/Li for Si-TFMA-Li/PEGDME-500.

For samples at different O/Li ratios, conductivity data smoothly increases with increase of temperature. For sample with O/Li of 32, room temperature value gives the highest conductivity of all samples. The room temperature conductivity VS. O/Li ratio plot shows an increase in conductivity with the increase of O/Li ratio. After reaching a peak value of 10^{-6} S/cm at an O/Li of 32, the conductivity decreases. As the particle content increases, the PEGDME-500 and particle mixture becomes inhomogeneous, particle could not get well dispersed, this only results in worse conductivity. Minimizing the volume fraction of the silica cores, i.e., increasing the molecular weight of the polyelectrolytes attached to the particles is the key issue to improve the physical attributes of the electrolyte. An alternative approach is to increase the number of lithium carriers in each monomer unit.

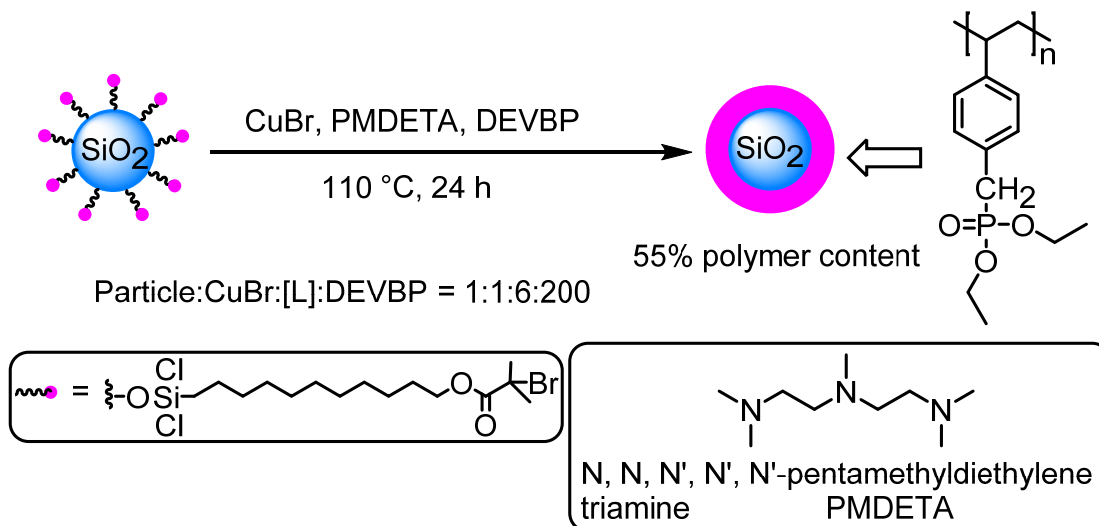
2.4. Phosphonic acid modified particles

To improve the conductivity, we used a styryl phosphonate which is a precursor to polymers with phosphonic acid as the repeating unit. Once lithiated, each repeating unit would have two lithium cations, and increase the local lithium cation density on the particles. To avoid the potential influence of the phosphonic acid on the ATRP initiating system, we used a phosphonate ester as the monomer, the ester group was hydrolyzed after polymerizing the styryl phosphonate on the particle surface.



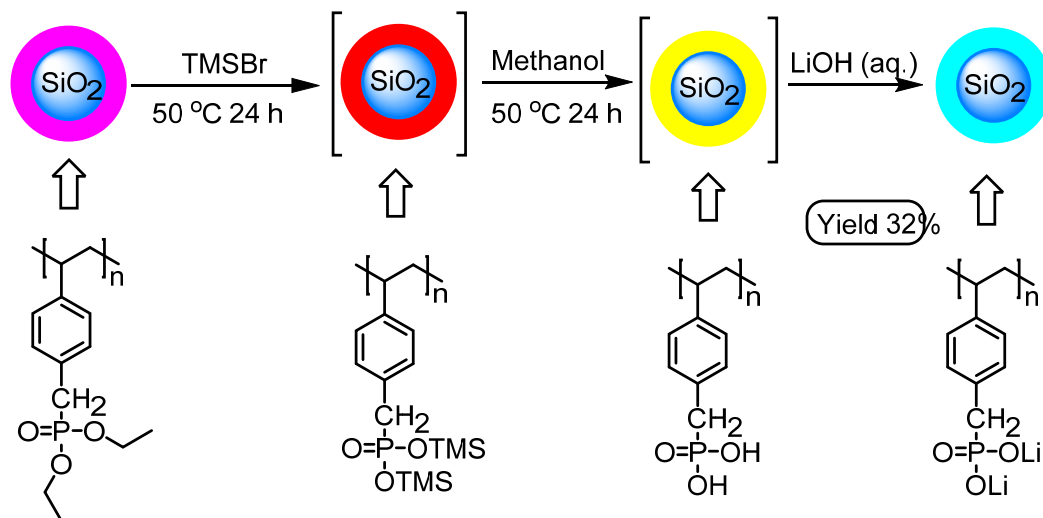
Scheme 19. Synthesis of diethyl 4-vinylbenzylphosphonate (DEVBP).

We used a modified version of Chidsey's protocol⁶² for the synthesis of diethyl 4-vinylbenzylphosphonate (DEVBP). Our initial attempts suffered from low yields. Since the benzyl iodide intermediate was light sensitive, we decided to add the triphenyl phosphite without isolating the 4-iodomethyl styrene intermediate. From this one-pot variation, we isolated the desired product in 55 % yield (Scheme 19).



Scheme 20. ATRP of diethyl 4-vinylbenzylphosphonate (DEVBP) on particle surface.

ATRP of DEVBP on silica particle surface used PMDETA as ligand with a metal ligand ratio of 1:6, the reaction normally continues for 24 h before work-up (Scheme 20). This polymerization chemistry was done 20 times or so to get enough material for characterization. Only the first trial gave a polymer content of more than 70 wt%, samples typically have polymer content of 50 wt%, these sample were used for lithiation and conductivity measurement.



Scheme 21. Lithiation procedure for poly(diethyl 4-vinylbenzylphosphonate) grafted silica particle (Si-PDEVBP).

The monomer, diethyl 4-vinylbenzylphosphonate, was used as a model compound to establish suitable conditions for the hydrolysis of the phosphonate ester. Refluxing in 4 M HCl or 2 M NaOH, failed to hydrolyzed product. In a two-step reaction, the phosphonate was treated with TMSCl, followed by methanolysis. However, the procedure of Mullen,⁶³ using TMSBr followed by methanolysis, successfully converted the phosphonate ester to the acid (Scheme 21). The lithium content in Si-PPLi was 3.5×10^{-2} g Li/g sample. With two lithium atoms in one repeating unit, lithium content increases. With this relatively high lithium content, we could get a high lithium concentration with less particle content, this could potentially increase the conductivity of the electrolytes.

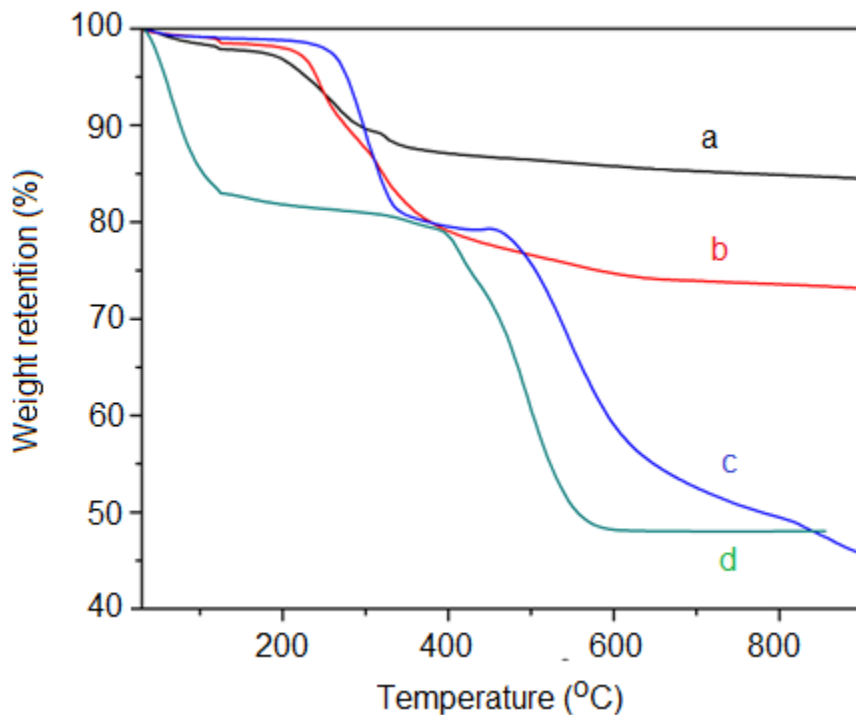


Figure 23. TGA curves of (a) Snowtex-S silica particles; (b) Si-Initiator, initiator grafted silica particle; (c) Si-PDEVBP, silica particle grafted by poly(diethyl 4-vinylbenzylphosphonate); (d) Si-PPLi, poly(lithium 4-vinylbenzylphosphonate).

Figure 23 shows TGA curves of silica particles at different stages. Curve c and d proved successful ATRP of diethyl 4-vinylbenzylphosphonate monomer on particle surface.

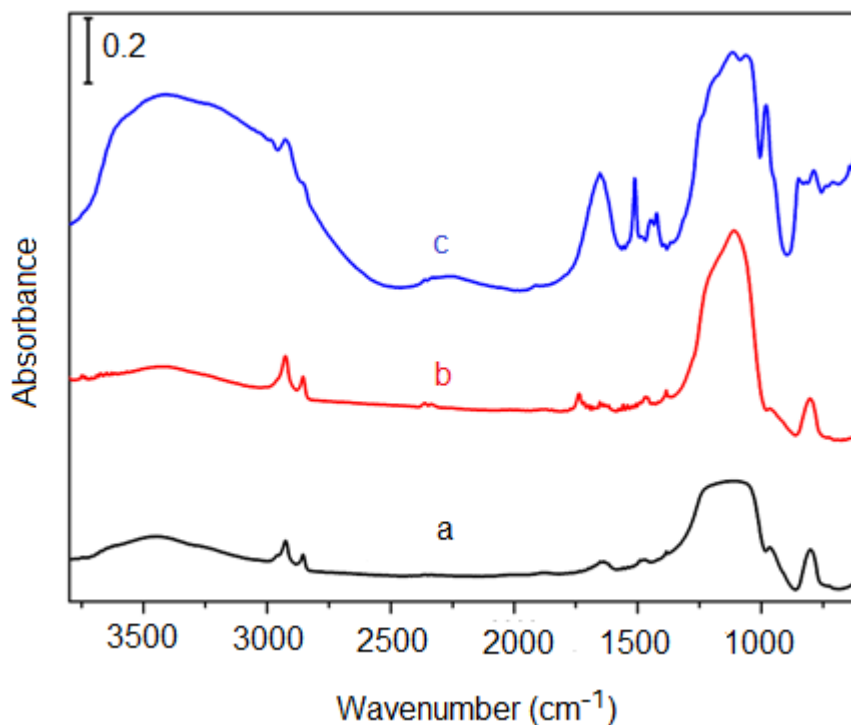


Figure 24. FTIR spectra of (a) Snowtex-S silica particles; (b) Si-Initiator, initiator grafted silica particles; (c) Si-PPLi, silica particle grafted by poly(lithium 4-vinylbenzylphosphonate).

In curve c Figure 24, the very strong peak at $960\text{-}1300\text{cm}^{-1}$ was assigned to P=O stretching. The out-of-plane CH bending at 817 cm^{-1} is characteristic of the para-substituted benzene rings, expected for the styrene moiety, confirming the successful growth of the polymer from the surface.

O/Li ratio	32	64	96	128	192	256
Particle content (wt%)	12.6	6.7	4.6	3.5	2.3	1.8

Table 9. Particle weight content for electrolytes prepared from Si-PPLi (3.45×10^{-2} g Li/g sample) dispersed in PEGDME-500.

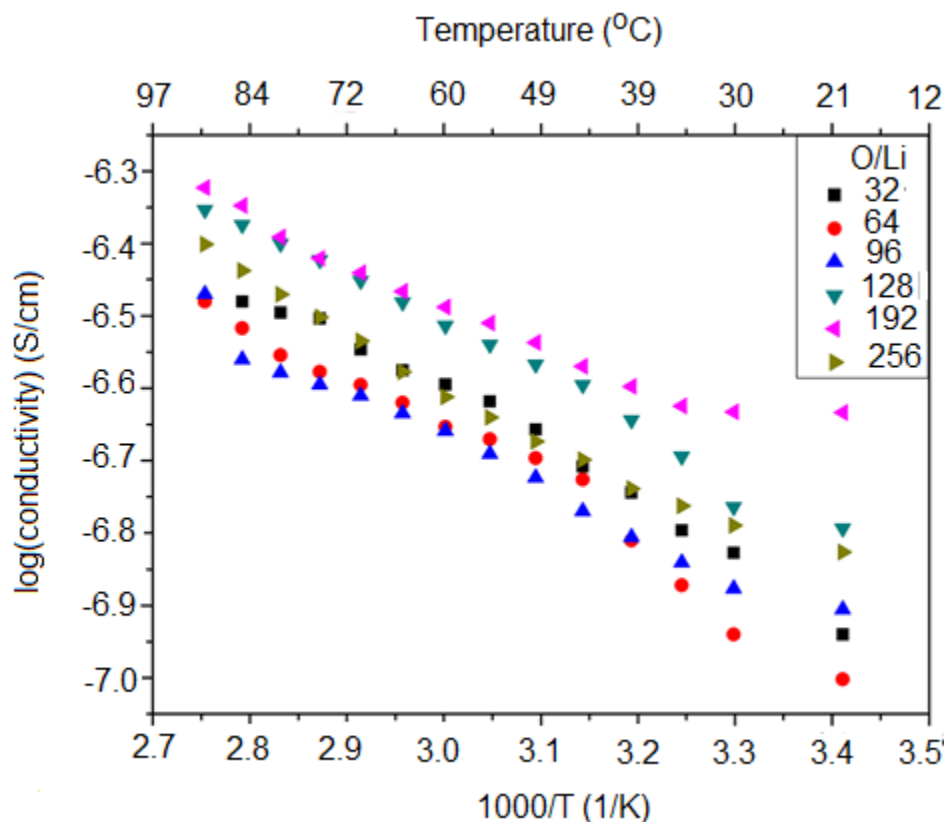


Figure 25. Temperature dependent conductivity for Si-PPLi/PEGDME-500 at various O/Li ratios.

Figure 25 shows conductivity change with the increase of temperature for Si-PPLi mixed with PEGDME-500, conductivity increases with temperature for all samples. Samples with six different O/Li ratios were characterized, particle content reaches 13 wt% at O/Li ratio of 32. In different sets of samples, conductivity at O/Li 32 were lower than those at O/Li 64, further increase of particle content was not tried.

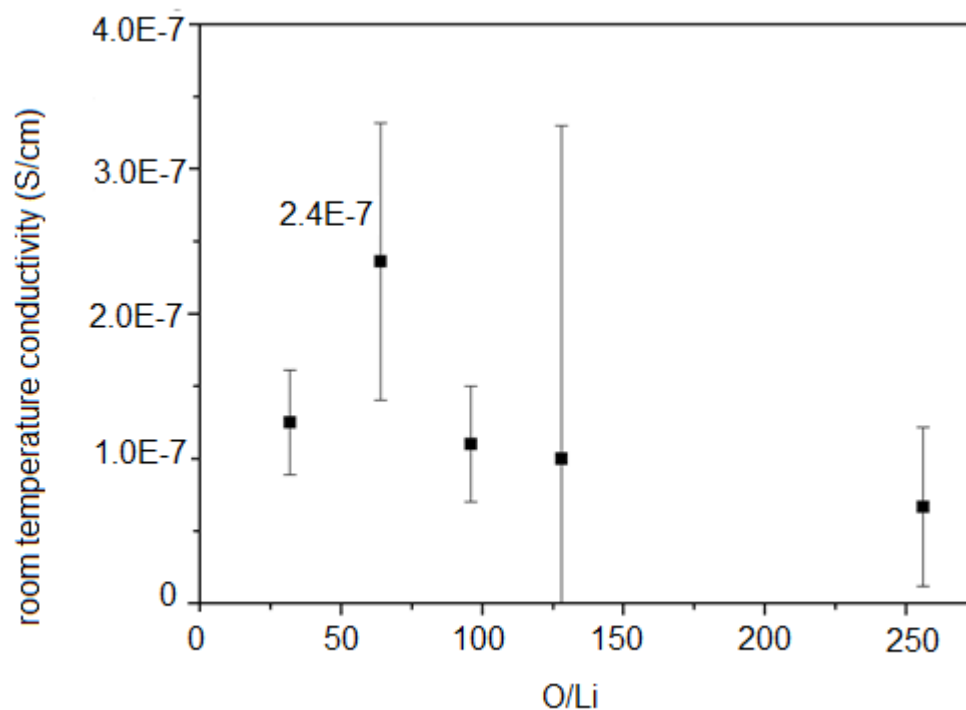


Figure 26. Room temperature conductivity vs. O/Li for Si-PPLi/PEGDME-500.

Room temperature conductivity reaches peak value of 2.4×10^{-7} S/cm at O/Li of 64 (Figure 26). Conductivity of Si-PPLi is not evidently improved, probably because the low degree of dissociation between lithium cation and the phosphonate group. The low dissociation degree between two counterions sacrificed increase of lithium content, free moving lithium cations in the materials were not increased, conductivity was not improved.

In this project, we aimed at developing single lithium ion electrolytes based on polymer modified silica nanoparticles, conductivity data show that different polymer structure gave different properties, a TFSI analogue monomer gave the best conductivity. However, at this point, there are several measurements we need to do in the near future:

- 1) People have been using ATRP chemistry to modify silica nanoparticles, characterization of the polymer content on particle surface was done using hydrofluoric acid to etch the particle, extracting the polymer content to organic (toluene) phase. This polymer solution could be subject to GPC to get related data. Kinetics of surface ATRP could be done using the same protocol. However, most of the previous work used styrene or methyl methacrylate as monomer, in their case the polymer has a good distribution in the organic phase. In our case, the polymer electrolytes are quite soluble in water solution, it is difficult to extract the polymer content to organic phase, NMR spectra from the organic phase were quite messy at this point;
- 2) To prove the single-ion concept, lithium transference number will be measured. The electrolyte in this work is composed of PEGDME-500 and polymer grafted particle. PEO is basically non-conductive, anions were covalently bonded on particle surface, lithium cation is the only conductive ion in the materials, the lithium transference number is supposed to be close to unity.

3. Conclusion

Four different monomer structures were grown on silica nanoparticles using ATRP. The first monomer, sodium 4-styrenesulfonate was a commonly used precursor for lithium single ion electrolyte; by intramolecularly incorporating a

PEO containing monomer, it was aimed to improve lithium cation conducting behavior and interfacial property between particles and PEGDME-500; the third monomer featured a trifluoromethane sulfonic imide structure, which could give higher dissociation degree between anion and lithium cation; in the fourth monomer, each phosphonate group contained two lithium cations, this was supposed to increase the lithium content. In each case, the polymer content on particles was more than 50 wt%. These particles were post-grafted to lithium conductor, and mixed with PEGDME-500 oligomer. This protocol gave high polymer content and relatively high lithiation efficiency, which resulted in a high lithium content. Room temperature conductivity of these materials were normally in the range of 10^{-7} to 10^{-6} S/cm.

4. Experimental Section

4.1. Materials

Lithium hydroxide monohydrate (Aldrich, 98%), cetyltrimethylammonium bromide (CTAB, Aldrich), 4-styrenesulfonic acid sodium salt hydrate (Aldrich), trifluoromethanesulfonic anhydride (Aldrich, 99%), bromotrimethylsilane (Alfa Aesar, 97%), butyllithium, 2.5 M solution in hexane (Aldrich), 4-vinylbenzyl chloride (Aldrich, 90%), triethyl phosphite (Aldrich, 98%), ethanolamine (Aldrich, 99%), thionyl chloride (CCI, 99.7%), methacryloyl chloride (Aldrich, 97%), triethylamine (J. T. Baker), hydroquinone (J. T. Baker Chemical), I chloride (J. T. Baker Chemical), sodium thiosulfate (CCI), Sodium Iodide (Jade Scientific), N, N,

N', N', N''-pentamethyldiethylenetriamine (PMDETA, Aldrich, 99%) were used as received. Cu(I)Br (Aldrich, 99.999%) was purified using saturated aqueous NaBr solution. Bipyridine (Aldrich, 99%) was recrystallized from hexane and sublimed. Poly(ethylene glycol) methyl ether methacrylate (Average M_n 1,100, Aldrich) was passed through a basic column before use. Snowtex-S (7-10 nm) were received as a gift from Nissan Chemical.

4.2. Characterization

^1H NMR and ^{13}C NMR spectra were collected using a Varian UnityPlus-500 spectrometer in CDCl_3 with the residual proton signals from the solvent as the chemical shift standard. Thermogravimetric analysis (TGA) were carried out in air on Perkin-Elmer TGA 7 instruments at heating rate of $10\text{ }^\circ\text{C}/\text{min}$. Sample were held at $120\text{ }^\circ\text{C}$ for 30min before starting the heating process. FTIR spectra were collected in a Mattson Galaxy 300 spectrometer. FTIR samples were made by mixing with KBr, grounded and pressed to pellets. A JEOL-100CX transmittance electron microscope was used to detect the microstructure of the particles. Particles were dispersed in Mili-Q water using ultrasonication at low concentration. A drop of this suspension was put onto a carbon-coated copper mesh grid. Excess of water was absorbed carefully by filter paper and then air dried. Conductivity data were collected from an HP 4192A LF Impedance Analyzer scanning from 5 Hz to 13 MHz with an applied voltage of 10 mV. Sample cell uses

two steel disks as symmetrical electrodes, containing sample of 0.61 cm in radii and 0.0175 cm in thickness. Polymer grafted particle were finely ground using a pestle and mortar then transferred into glovebox. PEGDME-500 was passed through a basic column and diluted with ether. The solution was stirred with molecular sieves for 24 h before removing solvent on rotovac and put onto vacuum line at 50 °C for 24 h. Purified PEGDME-500 was transferred into glovebox. For different O/Li particles were mixed with 0.2 g PEGDME-500 and stirred in 8ml vial for 24 h to make it well dispersed. Data were taken at r.t., 30, 35, 40, 45, 50, 55, 60, 65, 70, 75, 80, 85, 90 °C. Samples were equilibrated at each temperature for at least 10 minutes before measurement. Sample cell was constructed of stainless steel disks separated by a Teflon collar.

Lithium quantitative analysis was done using Varian 710-ES ICP Optical Emission Spectrometer under argon atmosphere. Six standard solutions (LiCl concentration of 0, 0.05, 0.5, 1, 2, 4.5 ppm, 2 wt% HNO₃ for each solution) were used to make working curve for each measurement. Peaks at wavelength of 460.289 nm, 670.783 nm, 610.365 nm were all used for data collection, results showed that data from the three different emission peaks were consistent. Following are data from wavelength of 670.783 nm, **calibration solution concentration/ppm (instrument peak intensity):**

0 (22457), 0.05 (187440.0), 0.5 (1958228.6), 1 (3490400.0), 2 (8897000.0), 4.5

(15000000.0), Si-PSSLi (6704000.0) mass of sample 6.583 mg, 2.40×10^{-2} g Li/g sample.

0 (22457), 0.05 (187440.0), 0.5 (1958228.6), 1 (3490400.0), 2 (8897000.0), 4.5 (15000000.0), Si-PSSLi-PEGMA (5581714.3) mass of sample 8.480 mg, 1.56×10^{-2} g Li/g sample.

0 (18606.4), 0.05 (75106.4), 0.5 (368117.0), 1 (548085.1), 2 (1106914.9), 4.5 (2336170.2), Si-TFMA-Li (6123404.3), mass of sample 7.953 mg, 2.00×10^{-2} g Li/g sample.

0 (22542.9), 0.05 (182800.0), 0.5 (1954857.1), 1 (3460800.0), 2 (8737000.0), 4.5 (14800000.0), Si-PPLi (5407978.7), mass of sample 3.777 mg, 3.45×10^{-2} g Li/g sample.

4.3. Synthesis

ATRP of sodium 4-styrene sulfonate with Snotex-S particle: In a 50 mL Schlenk flask, 1.72 g 4-styrene sulfonate (8.35 mmol), 56 mg bipyridine (0.32 mmol), 6 mL Mili-Q water and 2 mL methanol was mixed, which was charged with a magnetic stir bar to stir to be a clear solution, 0.124 g initiator grafted silica particle was added and the mixture was ultrasonicated for 15 mins. After 3 cycles of Freeze-Pump-Thaw, the Schlenk flask was filled with nitrogen and 17.2 mg CuBr was added. After another cycle of Freeze-Pump-Thaw, the reaction was done under room temperature for 12 hours. To work up the reaction, Schlenk flask was open to air, the mixture was transferred to 50 mL centrifuge tube and washed

with MilliQ water twice, N,N,N',N'-ethylenediaminetetraacetic acid (disodium salt dehydrate, EDTA·2Na) saturated solution 3 times, Milli-Q water once. In each step the polymer grafted silica particle was recovered using centrifuge. The product was put onto vacuum line dried at 90 °C overnight.

Lithiation of Poly(4-styrene sulfonate) grafted silica particle: In a 250 mL flask, 2.4 g lithium chloride was dissolved in 100 mL Milli-Q water. 0.32 g poly(4-styrene sulfonate) grafted silica particle was added in the solution and ultrasonicated 15 min before reaction at room temperature for 48 h. Product was collected by centrifuge and washed by Milli-Q water 3 times. It was dried under vacuum at 90 °C overnight.

Synthesis of ethanolamine hydrochloride and aminoethylmethacrylate hydrochloride followed the procedure adapted from Forcada's work with slight modification. 10 mL ethanolamine was dissolved with 250 mL ethanol in an 500 mL Erlenmeyer flask on ice bath. Thionyl chloride was added dropwise using pipet until no smoke generated. The suspension was stirred for another 10 minutes with ice bath, the white crystals were collected by filtration and washed with hexane. The product was air dried and 15.7 g product was obtained (yield 97%).

Synthesis of aminoethylmethacrylate hydrochloride: In a 250 mL 3-neck flask, 6.5 g ethanolamine (67 mmol) hydrochloride and 0.05 g hydroquinone (0.45 mmol) was mixed. The mixture was heated up to 95 °C for 20 minutes with magnetic stirring until the salt melted. 10 mL methacryloyl chloride (96 mmol) was added by

syringe over a period of 20 mins. The temperature was increased to 115 °C for 2 hours, then decreased to 65 °C, 200 mL ethyl acetate was added while the reaction mixture was still at molten state. White precipitant was produced and collected by filtration. 7.85 g product was obtained (yield 72%).

Synthesis of trifluoromethane sulfonic aminoethylmethacrylate: In a 100 mL flask, 0.57 g aminoethylmethacrylate hydrochloride (3.43 mmol), 0.6 g triethylamine (5.94 mmol), and 20mL chloroform was mixed. The mixture was put onto acetonitrile/dry ice bath (-45 °C). Using syringe to add 8 ml trifluoromethane sulfonic anhydride (4.76 mmol). After addition of Tf₂O was over, CH₃CN/dry ice bath was removed and the reaction was under room temperature for another 2 hours. 30 mL saturated NaHCO₃ solution was added to the reaction mixture, which was extracted by 3*30 mL dichloromethane. The organic layer was washed with 2 x 50 mL 2 M HCl solution, and further wash with 2 x 30 mL brine. MgSO₄ was used to dry the dichloromethane solution and condensed on rotovac. 0.6 g product was obtained (yield 67%).

ATRP of trifluoromethane sulfonic aminoethylmethacrylate with Snotex-S particle: In a Schlenk flask, 0.62 g 4-vinylbenzylphosphonate (2.36 mmol), 62.3 mg N,N,N',N',N''- -Pentamethyldiethylenetriamine (PMDETA 0.36 mmol), 5 mL DMF and 62 mg initiator grafted particle was mixed and ultrasonicated for 15 mins. After 3 cycles of Freeze-Pump-Thaw, the Schlenk flask was filled with nitrogen and 8.6 mg CuBr (0.06 mmol) was added. After another cycle of

Freeze-Pump-Thaw, the reaction was done at 90 °C for 12 hours. To work up the reaction, Schlenk flask was open to air, the mixture was transferred to 50 mL centrifuge tube and washed with DMF twice, EDTA·2Na saturated solution 3 times, MiliQ water once. In each step the polymer grafted silica particle was recovered using centrifuge. The product was put onto vacuum line dried at 90 °C overnight.

Lithiation of poly(trifluoromethane sulfonic aminoethylmethacrylate)

grafted particles (Si-TFMA to Si-TFMA-Li) In a 200 mL round bottom flask, 1 g Si-TFMA was dispersed in 150 mL dry toluene, 1 mL *n*-BuLi hexane solution (2.5 M) was added slowly in to the suspension. It was stirred overnight at r.t. and product recovered by centrifuge. It was washed three times with toluene and three times with acetone, dried under vacuum at 90 °C overnight.

Synthesis of trifluoromethane sulfonic octylamine

In a 100 mL round bottom flask, 2.58 g octylamine (0.02 mol), 3.03 g triethylamine (0.03 mol) and 30 mL dry dichloromethane were added. The mixture was placed onto a -78 °C cold bath under nitrogen, temperature of the cold bath was monitored using a low temperature thermometer. 4 mL of trifluoromethane sulfonic anhydride (1.2 equiv.) was slowly added over 15min. After addition of the anhydride was over, cold bath was removed, the reaction was performed overnight under nitrogen atmosphere. To work up the reaction, 30 mL saturated NaHCO₃ solution was added to the reaction mixture, which was extracted by 3 x 30 mL dichloromethane. The organic layer was washed with 2 x 50 ml 2 M HCl solution, and further wash with 2 x 30

mL brine. MgSO_4 was used to dry the dichloromethane solution and condensed on rotovac. To separate the mono TFSI amine from bi TFSI amine, the crude product was added to THF solution of potassium *t*-butoxide (2 equiv.), the mixture was stirred for 5 h and solvent removed on rotovac. Concentrated HCl was added and the mixture was extracted with dichloromethane 3 x 50 mL. Organic layer was washed with water and dried over MgSO_4 . The solvent was removed and dried under vacuum line, giving the pure mono TFSI product.

Lithiation of trifluoromethane sulfonic octylamine A 100 mL round bottom flask was flame dried before use, 1.3 g of trifluoromethane sulfonic octylamine (5 mmol) and 30 mL dry THF was added under nitrogen. 3 mL *n*-BuLi hexane solution (2.5 M) was added slowly to the solution, It was stirred overnight at r.t. and solvent was removed under rotovac and dried under vacuum line.

Synthesis of diethyl 4-vinylbenzylphosphonate followed procedure in a paper from Chidsey and coworkers, with a slight modification. 10.5 g NaI (70.4 mmol) and 50 mL methyl ethyl ketone were mixed in an Aluminum foil wrapped 250 mL round bottom flask, the suspension was purged with nitrogen for 30 mins. 2.5 mL (14.1 mmol, 90%) vinyl benzyl chloride was added by syringe. It was reacted at room temperature for 8 hours under nitrogen atmosphere. 2.4 g triethyl phosphite was added, the flask was put onto 90 °C oil bath for additional 7 hours. Solvent and ethyl iodide by-product were removed on rotovap. Crude product was dissolved in 300 mL diethyl ether, which was washed with 3 x 150 mL DI water.

The organic layer was dried by MgSO₄. The ether solution was condensed and purified by flash column (hexane/EtOAc=1:1) to give 1.97 g product (yield 55%).

¹H NMR (500 MHz, CDCl₃, ppm): δ 4.46 (s, 2 H), 5.26 (d, 1 H), 5.75 (d, 1 H), 6.68 (d of d, 1 H), 7.34 (s, 4H).

ATRP of 4-vinylbenzylphosphonate with Snotex-S particle: In a Schlenk flask, 0.6 g 4-vinylbenzylphosphonate (2.36 mmol), 62.3 mg N,N,N',N',N''-Pentamethyl-diethylenetriamine (PMDETA 0.36 mmol), 5 mL DMF and 62 mg initiator grafted particle was mixed and ultrasonicated for 15 mins. After 3 cycles of Freeze-Pump-Thaw, the Schlenk flask was filled with nitrogen and 8.6 mg CuBr (0.06 mmol) was added. After another cycle of Freeze-Pump-Thaw, the reaction was done at 90 °C for 12 h. To work up the reaction, Schlenk flask was open to air, the mixture was transferred to 50 mL centrifuge tube and washed with DMF twice, EDTA·2Na saturated solution 3 times, Mili-Q water once. In each step the polymer grafted silica particle was recovered using centrifuge. The product was put onto vacuum line dried at 90 °C overnight.

Lithiation of poly(4-vinylbenzylphosphonate) grafted silica particle (Si-PDEVBP to Si-PPLi) in a 500 mL round bottom flask, 1 g Si-PDEVBP was dispersed in 200 mL dry dichloromethane by ultrasonication, 0.7 mL TMSBr (5.3 mmol) was injected into the solution. The solution was stirred at 50 °C for 24 h before removing the solvent on rotovac. 300 mL MeOH was added into the flask slowly, the suspension was ultrasonicated for another 10 min and put onto 50 °C

oil bath for 24 h. Solvent was removed on rotovac, 10 g lithium hydroxide monohydrate (0.24 mol) in 400ml Mili-Q water was added into the flask, ultrasonicated for 10 mins, and reacted at r.t. for 12 h. Product was recovered by centrifuge, washed ten times with large amount of Mili-Q water and dried at 90 °C under vacuum overnight.

REFERENCES

REFERENCES

- (1) Whittingham, M. S. *Science*, **1976**, *192*, 1126 -1127.
- (2) Guyomard, D.; Tarascon, J-M. *Adv. Mater.* **1994**, *6*, 408.
- (3) Ahmad, S. *Ionics*, **2009**, *15*, 309 -321.
- (4) Wright, P. V. *Br. Polymer J.*, **1975**, *7*, 319 -327.
- (5) Armand, M. B.; Chabagno, J. M.; Duclot, M. *Second International Meeting on Solid Electrolytes, St Andrews, Scotland, 20-22 Sept., 1978*, Extended Abstract.
- (6) Takahashi, Y.; Takadoro, H. *Macromolecules*, **1973**, *6*, 672-675.
- (7) Ratner, M. A.; Shriver, D. F. *Chem. Rev.* **1988**, *88*, 109-124.
- (8) Vogel, H. *Phys. Z.* **1921**, *22*, 645.
- (9) Tamman, G.; Hesse, W. *Z. Anorg. Allg. Chem.* **1926**, *156*, 245-257.
- (10) Fulcher, G. S. *J. Am. Ceram. Soc.* **1925**, *8*, 339-355.
- (11) Dias, F. B.; Plomp, L.; Veldhuis, J. B. J. *J. Power Sources*, **2000**, *88*, 169-191.
- (12) Evans, J.; Vincent, C. A.; Bruce, P. G. *Polymer*, **1987**, *28*, 2324-2328.
- (13) Lee, H. S.; Yang, X. Q.; McBreen, J.; Choi, L. S.; Okamoto, Y. *J. Electrochem. Soc.* **1996**, *143*, 3825-3829.
- (14) Lee, H. S.; Yang, X. Q.; Xiang C. L.; McBreen, J.; Choi, L. S.; *J. Electrochem. Soc.* **1998**, *145*, 2813-2818.

- (15) Lee, H. S.; Yang, X. Q.; Sun, X.; McBreen, J. *J. Power Sources* **2001**, 97-98, 566-569.
- (16) Blazejczyk, A.; Wieczorek, W.; Kovarsky, R.; Golodnitsky, D.; Peled, E.; Scanlon, L. G.; Appetecchi, G. B.; Scrosati, B. *J. Electrochem. Soc.* **2004**, 151, 1762-1766.
- (17) Blazejczyk, A.; Szczupak, M.; Wieczorek, W.; Cmoch, P.; Appetecchi, G. B.; Scrosati, B.; Kovarsky, R.; Golodnitsky, D.; Peled, E. *Chem. Mater.* **2005**, 17, 1535-1547.
- (18) Kalita, M.; Bukat, M.; Ciosek, M.; Siekierski, M.; Chung, S. H.; Rodriguez, T.; Greenbaum, S. G.; Kovarsky, R.; Golodnitsky, D.; Peled, E.; Zane, D.; Scrosati, B.; Wieczorek, W. *Electrochim. Acta*, **2005**, 50, 3942-3948.
- (19) Plewa, A.; Chylinski, F.; Kalita, M.; Bukat, M.; Parzuchowski, P.; Borkowska, R.; Siekierski, M.; Zukowska, G. Z.; Wieczorek, W. *J. Power Sources*, **2006**, 159, 431-437.
- (20) Mehta, M. A.; Fujinami, T.; *Solid State Ionics* **1998**, 113-115, 187-192.
- (21) Mehta, M. A.; Fujinami, T.; Inoue, T.; *J. Power Sources*, **1999**, 81-82, 724-728.
- (22) Mehta, M. A.; Fujinami, T.; Inoue, S.; Matsushita, K.; Miwa, T.; Inoue, T.; *Electrochim. Acta* **2000**, 45, 1175-1180.
- (23) Zhang, S. S.; Chang, Z.; Xu, K.; Angell, C. A.; *Electrochim. Acta* **2000**, 45, 1229-1236.

- (24) Sun, X. G.; Angell, C. A.; *Electrochim. Acta* **2001**, *46*, 1467-1473.
- (25) Xu, W.; Sun, X. G.; Angell, C. A.; *Electrochim. Acta* **2003**, *48*, 2255-2266.
- (26) Croce, F.; Appetecchi, G. B.; Perci, L.; Scrosati, B. *Nature* **1998**, *394*, 456-458.
- (27) Scrosati, B.; Croce, F.; Panero, S. *J. Power Sources*, **2001**, *100*, 93-100.
- (28) Johansson, P.; Ratner, M. A.; Shriver, D. F. *J. Phys. Chem. B* **2001**, *105*, 9016-9021.
- (29) Sun, X. G.; Reeder, C. L.; Kerr, J. B.; *Macromolecules*, **2004**, *37*, 2219-2227.
- (30) Sun, X. G.; Kerr, J. B.; *Macromolecules*, **2004**, *37*, 5133-5135.
- (31) Sun, X. G.; Kerr, J. B.; *Macromolecules*, **2006**, *39*, 362-372.
- (32) Ryu, S-W.; Trapa, P. E.; Olugebefola, S. C.; G-Leon, J. A.; Sadoway, D. R.; Mayes, A. M. *J. Electrochem. Soc.* **2005**, *152*, 158-163.
- (33) Sadoway, D. R., Huang, B.; Trapa, P. E.; Soo, P. P.; Bannerjee, P.; Mayes, A. M. *J. Power Sources*, **2001**, *97-98*, 621-623.
- (34) Trapa, P. E.; Acar, M. H.; Sadoway, D. R.; Mayes, A. M. *J. Electrochem. Soc.* **2005**, *152*, 2281-2284.
- (35) Trapa, P. E.; Reyes, A. B.; Gupta, R. S. D.; Mayes, A. M.; Sadoway, D. R. *J. Electrochem. Soc.* **2006**, *153*, 1098-1101.
- (36) Kurian, M.; Galvin, M. E.; Trapa, P. E.; Sadoway, D. R.; Mayes, A. M. *Electrochim. Acta* **2005**, *50*, 2125-2134.

- (37) Siska, D. P.; Shriver, D. F. *Chem. Mater.* **2001**, *13*, 4698-4700.
- (38) Snyder, J. F.; Ratner, M. A.; Shriver, D. F. *J. Electrochem. Soc.* **2003**, *150*, 1090-1094.
- (39) Snyder, J. F.; Hutchison, J. C.; Ratner, M. A.; Shriver, D. F. *Chem. Mater.* **2003**, *15*, 4223-4230.
- (40) Fujinami, T.; Tokimune, A.; Mehta, M. A.; Shriver, D. F.; Rawsby, G. C. *Chem. Mater.* **1997**, *9*, 2236-2239.
- (41) Ito, K.; Ohno, H. *Solid State Ionics* **1995**, *79*, 300-305.
- (42) Tominaga, Y.; Ohno, H. *Solid State Ionics* **1999**, *124*, 323-329.
- (43) Endo, T.; Matsumoto, K. *J. Polym. Sci. Part A: Polym. Chem.* **2010**, *48*, 3113.
- (44) Endo, T.; Matsumoto, K. *Macromolecules*, **2009**, *42*, 4580.
- (45) Kurian, M.; Galvin, M. E.; Trapa, P. E.; Sadoway, D. R.; Mayes, A. M. *Electrochimica Acta*, **2005**, *50*, 2125-2134.
- (46) Singhal, R. G.; Capracotta, M. D.; Martin, J. D.; Khan, S. A.; Fedkiw, P. S. *J. Power Sources*, **2004**, *128*, 247-255.
- (47) Riley, M.; Fedkiw, P. S.; Kha, S. A. *J. Electrochem. Soc.* **2002**, *149*, 667-674.
- (48) Zhang, X-W.; Khan, S. A.; Fedkiw, P. S. *Electrochem. Solid-State Lett.* **2004**, *7*, 361-364.
- (49) Zhang, X-W.; Fedkiw, P. S. *J. Electrochem. Soc.* **2005**, *152*, 2413-2420.

- (50) Zhang, H.; Zhang, X-W.; Shiue, E.; Fedkiw, P. S. *J. Power Sources*, **2008**, *177*, 561-565.
- (51) Nugent, J. L.; Moganty, S. S.; Archer, L. A. *Adv. Mater. Early View*, **2010**, DOI: 10.1002/adma.201000898.
- (52) Werne, T.; Patten, T. E. *J. Am. Chem. Soc* **2001**, *123*, 7497-7505.
- (53) Bombalski, L.; Min, K.; Dong, H.; Tang, C.; Matyjaszewski, K. *Macromolecules*, **2007**, *40*, 7429-7432.
- (54) Sunday, D.; C-Medina, S.; Green, D. L. *Macromolecules*, **2010**, *43*, 4871-4878.
- (55) Jiang, X.; Zhong, G.; Horton, J. M.; Jin, N.; Zhu, L.; Zhao, B. *Macromolecules*, **2010**, *43*, 5387-5395.
- (56) Yameen, B.; Kaltbeitzel, A.; Langer, A.; Muller, F.; Goesele, U.; Knoll, W.; Azzaroni, O. *Angew. Chem. Int. Ed.* **2009**, *48*, 3124-3128.
- (57) Qin, Y; 2009, PhD Dissertation, MSU.
- (58) Zhang, X-W.; Fedkiw, P. S. *J. Electrochem. Soc.* **2005**, *152*, 2413-2420.
- (59) Asfour, F. H.; 2004, PhD Dissertation, MSU.
- (60) Sander, L. C.; Wise, S. A., *J. Chromatogr.* **1984**, *316*, (DEC), 163-181.
- (61) Ue, M. *J. Electrochem. Soc.* **1994**, *141*, 3336-3342.
- (62) Dudek, S. P.; Skes, H. D.; Chidsey, C. E. D. *J. Am. Chem. Soc.* **2001**, *123*, 8033-8038.
- (63) Markova, D.; Kumar, A.; Klapper, M.; Mullen, K.; *Polymer*, **2009**, *50*,

3411-3421.